Exploring the effect of the pore size distribution on the streaming potential generation in saturated porous media, insight from pore network simulations

Damien Jougnot, Aida Mendieta, Philippe Leroy, Alexis Maineult

Exploring the effect of the pore size distribution on the streaming potential generation in saturated porous media, insight from pore network simulations

Damien Jougnot [1], **Aida Mendieta** [1], **Philippe Leroy** [2], **Alexis Maineult** [1]

[1]Sorbonne Université, CNRS, EPHE, UMR 7619 METIS, Paris, France

[2]BRGM, Water, Environment, and Ecotechnologies Department, Orléans, France

Key Points:

- We simulate streaming potentials for 2D networks with different pore size distributions
- The pore size distribution has a very restricted influence on electrokinetic coupling coefficients
- A recent effective excess charge density model accounts for all the pore size distributions

Corresponding author: Damien Jougnot, damien.jougnot@upmc.fr

Abstract

Understanding streaming potential generation in porous media is of high interest for hydrological and reservoir studies as it allows to relate water fluxes to measurable electrical potential distributions. This streaming potential generation results from an electrokinetic coupling due to the presence of an electrical double layer developing at the interface between minerals and pore water. Therefore, the pore sizes of the porous medium are expected to play an important role in the streaming potential generation. In this work we use 2D pore network simulations to study the effect of the pore size distribution upon this electrokinetic mechanism. Our simulations under well-controlled conditions allow a detailed study of the influence of a large range of permeabilities (from 10^{-16} to 10^{-10} m^2) for different ionic concentrations (from 10^{-4} to 1 mol L^{-1}). We then use and compare two different approaches that have been used over the last decades to model and interpret the generation of the streaming potential: the classical coupling coefficient or the effective excess charge density, which has been defined recently. Our results show that the four pore size distributions tested in the present work have a restricted influence on the coupling coefficient for ionic concentration smaller than 10^{-3} mol L^{-1} while it completely drives the behaviour of the effective excess charge density over orders of magnitude. Then, we use these simulation results to test an analytical model based on a fractal pore size distributions [*Guarracino and Jougnot*, 2018]. We show that this model predicts well the effective excess charge density for all the tested pore size distribution within its intrinsic limitations, that is, for a thin double layer compared to the pore size.

1 Introduction

Self-Potential (SP) is one of the oldest geophysical methods [*Fox*, 1830] and consists in measuring the naturally occurring electrical field at the surface of or within geological media. The SP signal results from the superposition of multiple sources coming from contributions of two main processes: the electrokinetic (EK) contribution (i.e., related to water flux) and the electrochemical contributions (i.e., related to ionic concentration, thermal gradient, or redox gradient). In this work we focus on SP signals generated by electrokinetic phenomena: the so-called streaming potential. Details on the possible contributions to the SP signal can be found in *Revil and Jardani* [2013] or *Jouniaux et al.* [2009], among other references.

The streaming potential has been the subject of numerous scientific studies over the last two centuries [since *Quincke*, 1859] and involved in many applications: from oil and gas reservoir exploration to more recent critical zone studies [e.g., *Revil et al.*, 1999a; *Jougnot et al.*, 2015]. In geological media, minerals and organic matter exhibit a charged surface (usually negative) that is compensated by an excess of charges in the pore water distributed in the so-called electrical double layer (EDL) surrounding these grains [e.g. *Hunter*, 1981]. These charges can be dragged by a water flow, generating a charge separation that in turn generates an electrical current and a resulting electrical potential distribution. Given the difficulty of directly measuring the water flow in geological media, relating this measurable electrical potential distribution to the water flux is therefore of interest for many reservoir or environmental applications [e.g., *Jouniaux et al.*, 2009; *Revil and Jardani*, 2013].

For more than a century, the classical approach to quantitatively relate the electrical potential field to the water flux (or to a hydraulic pressure field) has been achieved by the use of the EK coupling coefficient, C_{EK} (V Pa^{-1}),

$$C_{EK} = \frac{\partial V}{\partial P}\Big|_{\mathbf{J}=\vec{0}}, \tag{1}$$

where V is the electrical potential (V) and is P the water pressure (Pa), in the assumptions that the system is under a quasi-static equilibrium and that no external current $\mathbf{J}$ is injected into the medium. *Helmholtz* [1879] and *von Smoluchowski* [1903] proposed the so-called Helmholtz-Smoluchowski (HS) equation to determine C_{EK} from a limited amount of parameters:

$$C_{EK}^{HS} = \frac{\varepsilon_w \zeta}{\eta_w \sigma_w}, \tag{2}$$

where ε_w, σ_w, and η_w are the dielectric permittivity (F m^{-1}), the electrical conductivity (S m^{-1}), and the dynamic viscosity (Pa s) of the pore water, respectively. The ζ-potential, ζ (V), corresponds to the electrical potential at the shear plane in the EDL, which is the plane separating mobile and immobile water molecules [e.g. *Hunter*, 1981; *Leroy et al.*, 2012; *Li et al.*, 2016, Fig. 1]. The HS equation has been successfully used to predict streaming potential measurements in geological media [e.g., *Jouniaux and Pozzi*, 1995a; *Pengra et al.*, 1999]. It is interesting to note that the HS equation seems completely independent from the pore space geometry of the medium. However, there is a strong assumption in this model: the surface conductivity of the grains, σ_s (S m^{-1}), must be negligible compared to the pore water conductivity, that is $\sigma_s \ll \sigma_w$. When this is not the case, alterna-

tive formulas have been proposed by several researchers [e.g., *Morgan et al.*, 1989; *Revil et al.*, 1999b; *Glover and Déry*, 2010], taking into account surface conductivity and making some assumptions on the pore space geometry.

More recently, an alternative approach to quantify the streaming potential generation has been proposed, focusing on the excess charge effectively dragged by the water flow. To the best of the authors knowledge, the first occurrence of this approach in the literature in english is in *Kormiltsev et al.* [1998] and was later independently found by *Revil and Leroy* [2004]. This parameter is an alternative to the coupling coefficient and can easily be related to it by re-writing the water flow and electrical current equations [see *Kormiltsev et al.*, 1998, for the first derivation]

$$C_{EK} = -\frac{\hat{Q}_v k}{\sigma \eta_w}, \tag{3}$$

where σ and k are the electrical conductivity (S m^{-1}) and permeability (m^2) of the medium, respectively. Following the formalism of Revil and co-authors, we call $\hat{Q}_v$ the effective excess charge density (C m^{-3}). Note that it is called α in *Kormiltsev et al.* [1998].

Several studies have shown empirical evidence to prove that the effective excess charge density depends on the permeability of the porous media [*Titov et al.*, 2002; *Jardani et al.*, 2007; *Bolève et al.*, 2012], indicating that this parameter is strongly influenced by the petrophysical properties of the considered geological medium. It has been shown that the pore water chemistry, both the composition and the ionic concentration, also have a significant effect on $\hat{Q}_v$ [e.g., *Jougnot et al.*, 2012, 2015; *Cherubini et al.*, 2018].

Recently, *Guarracino and Jougnot* [2018] proposed an analytical model directly relating $\hat{Q}_v$ to the permeability, porosity, pore water chemistry (through the ionic concentration), and the ζ-potential. This closed-form equation was derived with the assumptions of a simple binary symmetric pore water electrolyte and pore radii much larger than the diffuse layer thickness. In order to achieve the derivation of this analytical solution, the authors based their approach on the use of tortuous capillaries and a fractal pore size distribution. Interestingly, the pore size distribution does not directly appear in the closed-form equation. *Guarracino and Jougnot* [2018]'s model performs very well with different SP datasets from laboratory measurements [*Pengra et al.*, 1999; *Glover and Déry*, 2010]. Note that *Soldi et al.* [2019] propose an extension of this model to partially saturated conditions.

Pore network simulations can be used as a numerical tool to predict the electrokinetic coupling coefficient, and consequently the effective excess charge density, for dif-

ferent pore size distributions. *Bernabé* [1998] proposed a pioneer work to model streaming potential in heterogeneous media. Based on this work, further investigations on coupling effects in charged media in 2 or 3D have been performed [e.g., *Brovelli and Cassiani*, 2010; *Obliger et al.*, 2014; *Zhang et al.*, 2015], mainly to evaluate the impact of the electrokinetic coupling on the permeability in microporous media.

In this work, we use a pore network numerical code based on the works of *Bernabé* [1998] and *Maineult et al.* [2018]. It allows for the prediction of the coupling coefficient, permeability, and formation factor of a 2D pore network with well-controlled pore size distributions, and therefore the effective excess charge density from Eq. 3. After presenting the theoretical framework for the electrokinetic phenomena and the numerical method that we implemented, we will (1) study the effect of the pore size distribution on the streaming potential generation and (2) check for the applicability of the *Guarracino and Jougnot* [2018] analytical model for the prediction of the effective excess charge density obtained for different pore size distributions.

2 Theory of streaming current generation

2.1 Governing equations

Streaming current generation in geological media can be described by the following macroscopic governing equations [e.g., *Sill*, 1983]:

$$\mathbf{J} = \sigma \mathbf{E} + \mathbf{J}_s, \tag{4}$$

$$\nabla \cdot \mathbf{J} = 0, \tag{5}$$

where $\mathbf{J}$ is the total current density (A m^{-2}), $\mathbf{E} = -\nabla V$ is the electrical field (V m^{-1}), and $\mathbf{J}_s$ is the source current density (A m^{-2}). In the absence of external current, that is when no current is injected into the medium, combining Eqs. (4) and (5) yields,

$$\nabla \cdot (\sigma \nabla V) = \nabla \cdot \mathbf{J}_s. \tag{6}$$

When considering only EK processes in the SP signals, the source current density (i.e., streaming current density) can then be expressed as,

$$\mathbf{J}_s = \sigma C_{EK} \nabla \left(P - \rho_w g z \right), \tag{7}$$

where ρ_w is the water density (kg m^{-3}), g is the gravitational acceleration (m s^{-2}), and z is the elevation (m). We call Eq. (7) the coupling coefficient approach.

As described in *Kormiltsev et al.* [1998], combining Eq. 3 and Darcy's equation [*Darcy*, 1856], we obtain the Darcy velocity:

$$\mathbf{u} = -\frac{k}{\eta_w}\nabla\left(P - \rho_w g z\right). \tag{8}$$

Including Eq. 8 in Eq. 7, one can obtain the streaming current density from the effective excess charge approach,

$$\mathbf{J}_s = \hat{Q}_v \mathbf{u}. \tag{9}$$

Combining Eqs. 6 and 9 allows relating the streaming potential distribution to the Darcy velocity, a variable of uttermost interest in hydrology or reservoir studies, through the medium conductivity and effective excess charge density:

$$\nabla \cdot (\sigma \nabla V) = \nabla \cdot \left(\hat{Q}_v \mathbf{u}\right). \tag{10}$$

2.2 Electrochemical properties

Most geological materials have a solid matrix made of components with charged surfaces (mostly minerals but also organic matter) in contact with water due to the hydroxilation of the surface sites and ion substitutions in the crystal [*Hiemstra and Van Riemsdijk*, 2006; *Leroy et al.*, 2013, 2015; *Li et al.*, 2016]. An EDL is formed at the pore surface to compensate the surface charge as the system "solid matrix plus pore water" must satisfy the electroneutrality principle [e.g., *Hunter*, 1981; *Leroy and Revil*, 2004]. As shown in Fig. 1, the surface charge Q_0 (C m^{-2}) is counterbalanced by charges in the EDL of the pore water: (1) by charges adsorbed in the compact Stern layer Q_β (often considered to have a negligible thickness, therefore expressed in C m^{-2}) and (2) by a distribution of charges in the diffuse layer $\bar{Q}_v$ (C m^{-3}). This yields

$$\frac{S_{sw}}{V_w}\left(Q_0 + Q_\beta\right) + \bar{Q}_v = 0, \tag{11}$$

where S_{sw} is the surface of the solid in contact with water (m^2) and V_w is the pore water volume (m^3). The term $\bar{Q}_v$ is called the excess charge density in the diffuse layer. We call co-ions and counter-ions the ions with the same and the opposite sign of the surface charge density, respectively. In typical silica rocks, under typical environmental conditions, surfaces are usually negatively charged; the co-ions and counter-ions are therefore anions and cations, respectively [e.g., *Sverjensky*, 2006].

The distribution of ions in the diffuse layer depends on the distribution of the microscopic (or local) electrical potential in the pores, ψ (V), which follows the Poisson equa-

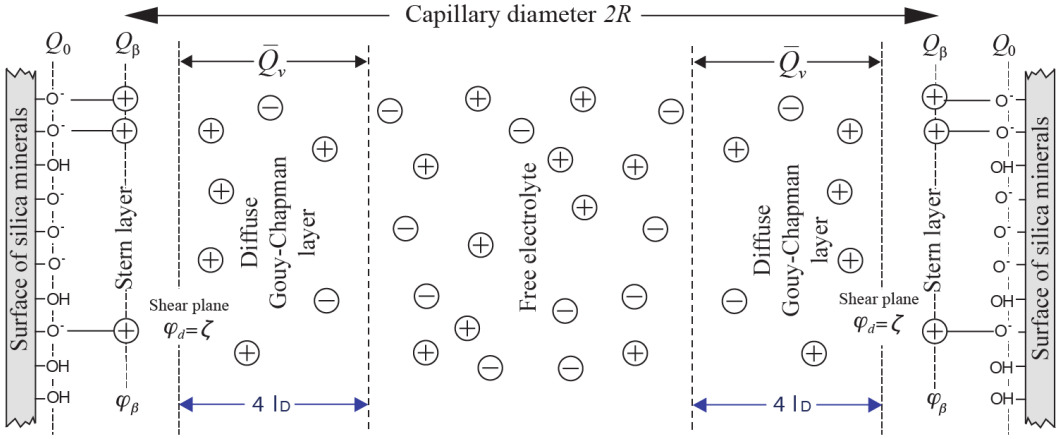

Figure 1. Scheme of the electrical double layer at the surface of silica minerals in contact with water for a given capillary radius R. l_D correspond to the Debye length (Eq. 18).

tion:

$$\nabla^2\psi = -\frac{\bar{Q}_v}{\varepsilon_w} \tag{12}$$

where ε_w is the dielectric permittivity of the pore water (F m^{-1}). We consider that the bulk pore water (i.e., the part of the electrolyte free from the effects of the charged surfaces) is an electrolyte composed of M ionic species i with a bulk concentration C_i^w (mol m^{-3}). The excess charge density in the diffuse layer is supposed to follow a Boltzmann distribution yielding:

$$\bar{Q}_v(r) = N_A \sum_{i=1}^{M} q_i C_i^w \exp\left(-\frac{q_i\psi(r)}{k_B T}\right) \tag{13}$$

where r is the distance from the shear plane (m) (that is the pore wall as we neglect the Stern layer thickness), $N_A = 6.022 \times 10^{23}$ mol^{-1} is the Avogadro's number, $k_B = 1.381 \times 10^{-23}$ J K^{-1} is the Boltzmann constant, T is the absolute temperature (K), and $q_i = \pm z_i e_0$ is the ion charge (C) which depends on its valency, z_i, and the elementary charge, $e_0 = 1.602 \times 10^{-19}$ C. Note that the extension of the diffuse layer corresponding to the fraction of the pore space in which the excess charge density is not negligible, can be approximated by a thickness equal to $4l_D$ (Fig. 1).

The excess charge density which is effectively displaced by the water flow is called effective or dynamic excess charge, depending on the authors, and symbolized as $\hat{Q}_v$ or $\bar{Q}_v^{eff}$ (C m^{-3}). It has to be distinguished from the other excess charge densities contained in the pore space [see the discussion in *Revil*, 2017]. The total excess charge density Q_v

(C m^{-3}), which includes all the charges of the EDL, is given by:

$$Q_v = \frac{S_{sw}}{V_w}\left(Q_\beta\right) + \bar{Q}_v = \rho_s\left(\frac{1-\phi}{\phi}\right)e_0 N_A CEC, \tag{14}$$

where CEC is the cationic exchange capacity (meq kg^{-1}), ϕ is the porosity, and ρ_s is the solid grain density (kg m^{-3}). Note that the CEC of hydroxide minerals such as quartz strongly depends on the pH and salinity [*Leroy et al.*, 2013]. As discussed in *Jougnot et al.* [2012], the excess charge density of the diffuse layer $\bar{Q}_v$ (Fig. 1) is usually considerably smaller than the total excess charge density Q_v and larger than the effective excess charge density $\hat{Q}_v$:

$$\hat{Q}_v \ll \bar{Q}_v \ll Q_v. \tag{15}$$

This is due to the fact that the effective excess charge density is weighted by the pore water velocity distribution through the pore (Fig. 10a). This concept is described in detail in *Jougnot et al.* [2012] and called "flux-averaging" in opposition to the "volume-averaging" up-scaling technique described in *Revil et al.* [2007].

2.3 Electrokinetic coupling at the pore scale

Following the capillary-based approaches proposed by *Jackson* [2008, 2010] and *Linde* [2009], *Jougnot et al.* [2012] consider the porous medium as a bundle of capillaries to develop the flux-averaging up-scaling procedure. The effective excess charge density $\hat{Q}_v^R$ dragged by the water flow in a single tube of radius R (m) is defined by:

$$\hat{Q}_v^R = \frac{\int_{r=0}^{R} \bar{Q}_v(r)v(r)dr}{\int_{r=0}^{R} v(r)dr}, \tag{16}$$

where $v(r)$ is the pore water velocity across the capillary (m s^{-1}).

In order to propose an analytical solution for Eq. (16), *Guarracino and Jougnot* [2018] consider the Debye-Hückel approximation, an usual way to derive analytically the distribution of the local electrical potential [e.g., *Jougnot et al.*, 2012, 2015; *Guarracino and Jougnot*, 2018; *Soldi et al.*, 2019]. This approximation is an accurate solution of the Poisson-Boltzmann equation (Eq. 12) for low local electrical potentials, i.e., $|\zeta| << (k_B T)/|q_i| \simeq 25$ mV (for T= 298 K) and monovalent ions. The microscopic electrical potential distribution in the diffuse layer of a NaCl pore water solution can then be expressed as,

$$\psi(r) = \zeta \exp\left(-\frac{r}{l_D}\right), \tag{17}$$

where l_D is the Debye length (m) defined as,

$$l_D = \sqrt{\frac{\varepsilon_w k_B T}{2 e_0^2 C^w N_A}}. \tag{18}$$

Note that this is a solution obtained for a flat surface [e.g., *Hunter*, 1981]. Nevertheless, it can be used for large pores, that is for a small curvature compared to the diffuse layer thickness [see discussion in *Jougnot et al.*, 2012; *Thanh*, 2018]. For a NaCl solution, Eq. (13) becomes,

$$\bar{Q}_v(r) = N_A e_0 C^w_{NaCl} \left[e^{-\frac{e_0 \psi(r)}{k_B T}} - e^{\frac{e_0 \psi(r)}{k_B T}} \right]. \tag{19}$$

Then the exponential terms of Eq. (19) are approximated by a four-term Taylor series:

$$e^{\pm \frac{e_0 \psi(r)}{k_B T}} = 1 \pm \frac{e_0 \psi(r)}{k_B T} + \frac{1}{2} \left(\frac{e_0 \psi(r)}{k_B T} \right)^2 \pm \frac{1}{6} \left(\frac{e_0 \psi(r)}{k_B T} \right)^3. \tag{20}$$

Substituting Eq. (20) in Eq. (19) and solving (16) considering a Poiseuille flow, it yields:

$$\begin{aligned}
\hat{Q}_v^R = \; & -\frac{8 N_A e_0^2 C^w_{NaCl} \zeta}{k_B T (R/l_D)^4} \left\{ 6 - e^{-\frac{R}{l_D}} \left[\left(\frac{R}{l_D} \right)^3 + 3 \left(\frac{R}{l_D} \right)^2 + 6 \left(\frac{R}{l_D} \right) + 6 \right] \right\} \\
& + \frac{24 N_A e_0^2 C^w_{NaCl} \zeta}{k_B T (R/l_D)^3} \left\{ 2 - e^{-\frac{R}{l_D}} \left[\left(\frac{R}{l_D} \right)^2 + 2 \left(\frac{R}{l_D} \right) + 2 \right] \right\} \\
& - \frac{16 N_A e_0^2 C^w_{NaCl} \zeta}{k_B T (R/l_D)^2} \left\{ 1 - e^{-\frac{R}{l_D}} \left[\left(\frac{R}{l_D} \right) + 1 \right] \right\} \\
& - \frac{4 N_A e_0^4 C^w_{NaCl} \zeta^3}{3 (k_B T)^3 (3R/l_D)^4} \left\{ 6 - e^{-\frac{3R}{l_D}} \left[\left(\frac{3R}{l_D} \right)^3 + 3 \left(\frac{3R}{l_D} \right)^2 + 6 \left(\frac{3R}{l_D} \right) + 6 \right] \right\} \\
& + \frac{4 N_A e_0^4 C^w_{NaCl} \zeta^3}{(k_B T)^3 (3R/l_D)^3} \left\{ 2 - e^{-\frac{3R}{l_D}} \left[\left(\frac{3R}{l_D} \right)^2 + 2 \left(\frac{3R}{l_D} \right) + 2 \right] \right\} \\
& - \frac{8 N_A e_0^4 C^w_{NaCl} \zeta^3}{3 (k_B T)^3 (3R/l_D)^2} \left\{ 1 - e^{-\frac{3R}{l_D}} \left[\left(\frac{3R}{l_D} \right) + 1 \right] \right\}.
\end{aligned} \tag{21}$$

Considering the thin double layer assumption $l_D \ll R$, *Guarracino and Jougnot* [2018] simplify Eq. 21 to obtain the following analytical solution to predict the effective excess charge in a single capillary with a radius R,

$$\hat{Q}_v^R = \frac{8 N_A e_0 C^w_{NaCl}}{(R/l_D)^2} \left[-2 \frac{e_0 \zeta}{k_B T} - \left(\frac{e_0 \zeta}{3 k_B T} \right)^3 \right]. \tag{22}$$

This solution is considered valid for $R > 5 l_D$, see discussion in *Guarracino and Jougnot* [2018] (their Fig. 2) and in *Thanh* [2018]. Note that the rather simple Eq. (22) is influenced both by geometry (R), interface (ζ, l_D), and chemical properties (C^w_{NaCl}).

2.4 Electrokinetic coupling at the REV scale

In order to study the streaming potential generation in natural geological media, a second upscaling procedure has to be performed to go from $\hat{Q}_v^R$ to the effective excess charge density at the Representative Elementary Volume (REV) scale, $\hat{Q}_v^{REV}$. The flux-averaging approach proposed by *Jougnot et al.* [2012] yields,

$$\hat{Q}_v^{REV} = \frac{\int_{R_{min}}^{R_{max}} \hat{Q}_v^R v^R f_D dR}{\int_{R_{min}}^{R_{max}} v^R f_D dR}, \tag{23}$$

where v^R is the average pore water velocity (m s^{-1}) in capillaries having a radius R, and f_D is the capillary size distribution. Eq. 23 holds for any capillary size distribution. *Jougnot et al.* [2012] propose to determine f_D from the hydrodynamic curves of the considered porous medium. This can be accomplished by two approaches: one based on the water retention curve f_D^{WR}, the other based on the relative permeability curve f_D^{RP}. Both approaches require numerical simulation.

Guarracino and Jougnot [2018] recently proposed an analytical approach to determine $\hat{Q}_v^{REV}$ at the REV scale considering a fractal pore size distribution under water saturated conditions. They solve Eq. 23 with $\hat{Q}_v^R$ from Eq. 22. Their analytical developments, based on the Debye-Hückel approximation, yield the following rather simple formula,

$$\hat{Q}_v^{REV} = N_A e_0 C^w l_D^2 \left[-2\frac{e_0\zeta}{k_B T} - \left(\frac{e_0\zeta}{3k_B T} \right)^3 \right] \frac{1}{\tau^2} \frac{\phi}{k}. \tag{24}$$

where τ is the dimensionless hydraulic tortuosity of the medium. The above equation predicts the effective excess charge density in terms of both macroscopic hydraulic parameters (porosity, permeability, and tortuosity) and parameters of chemical or interfacial nature (ionic concentration, ζ-potential and Debye length). One can see that the fractal pore size distribution does not explicitely appear in Eq. 24, as it is included in the porosity and permeability terms. Indeed, when developping the analytical solution presented above (Eq. 24), all the information related to the pore space geometry (e.g., the fractal pore size distribution) was included in the definition of porosity and permeability [see *Guarracino and Jougnot*, 2018, for more details on the model development]. This model has been recently extended to partially saturated conditions by *Soldi et al.* [2019]. Note that *Thanh* [2018] proposed an expression similar to Eq. 24 but only valid for a single capillary radius instead of a distribution of radii.

While the *Guarracino and Jougnot* [2018] analytical solution proposes an explicit link between $\hat{Q}_v$ and the medium's permeability, numerous previous studies have shown an empirical relationship between these two parameters before [e.g., *Titov et al.*, 2002; *Jardani et al.*, 2007; *Bolève et al.*, 2012; *Cherubini et al.*, 2018]. Among these works, *Jardani et al.* [2007] propose the following empirical relationship

$$\log_{10}(\hat{Q}_v^{REV}) = A_1 + A_2 \log_{10}(k), \tag{25}$$

where $A_1 = -9.2349$ and $A_2 = -0.8219$ are constant values obtained by fitting Eq. 25 to a large set of experimental data that includes various lithologies and ionic concentrations. It has been widely used for SP [e.g. *Jardani and Revil*, 2009; *Linde et al.*, 2011;

Soueid Ahmed et al., 2014; *Roubinet et al.*, 2016] and seismoelectrics [e.g. *Jougnot et al.*, 2013; *Revil et al.*, 2015; *Monachesi et al.*, 2015] applications.

3 Streaming potential modeling in a 2D pore network

The present section describes the pore network model that we developed and used to simulate the streaming potential generation in synthetic porous media. We first describe the electrokinetic coupling at the capillary scale and then how the up-scaling is performed in 2D pore networks with different pore size distributions. Note that the simulations are based on the classical coupling coefficient approach (Eq. 7) and that the effective excess charge density is obtained from the numerical simulation results and Eq. 3.

3.1 Coupled transport equations in a single capillary

The pore network simulations consider the electrokinetic coupling occuring in capillaries (i.e., pores). Our numerical simulations are based on the numerical framework of *Bernabé* [1998], where the magnitudes of the hydraulic, Q (m^3 s^{-1}), and electrical, J (A s^{-1}), fluxes in a single capillary of radius R (m) and length l (m) are given by the following equations:

$$\begin{cases} Q = -\dfrac{\pi R^4}{8\eta_w}\dfrac{(P_u - P_d)}{l} + \dfrac{\pi\epsilon_w R^2\zeta}{\eta_w}\left(1 - \dfrac{2}{R^2\zeta}\displaystyle\int_0^R r\psi(r)dr\right)\dfrac{(V_u - V_d)}{l} \\ J = \dfrac{\pi\epsilon_w R^2\zeta}{\eta_w}\left(1 - \dfrac{2}{R^2\zeta}\displaystyle\int_0^R r\psi(r)dr\right)\dfrac{(P_u - P_d)}{l} \\ \qquad - \left[\dfrac{2\pi\epsilon_w^2}{\eta_w}\displaystyle\int_0^R r\left(\dfrac{d\psi(r)}{dr}\right)^2 dr + 2\pi\sigma_w\displaystyle\int_0^R r\cosh\left(\dfrac{ze\psi(r)}{k_B T}\right)dr\right]\dfrac{(V_u - V_d)}{l} \end{cases}, \quad (26)$$

where P is the hydraulic pressure, V is the electrical potential and where the subscripts u and d are for the up and down water pressure and electrical potential values, respectively. This set of equations is a fully coupled system taking into account the classical Poiseuille flow, Ohm's law, and both the electrofiltration (i.e., a water displacement generating an electrical field) and the electroosmotic (i.e., an electrical field generating a water displacement) couplings [e.g., *Nourbehecht*, 1963]. Eq. 26 can be condensed into,

$$\begin{cases} Ql = -\gamma^h(P_u - P_d) + \gamma^c(V_u - V_d) \\ Jl = \gamma^c(P_u - P_d) + \gamma^e(V_u - V_d) \end{cases}, \quad (27)$$

where γ^h is the modified hydraulic conductance (in m^4 Pa^{-1} s^{-1}), γ^e is the modified electrical conductance (in S m), and γ^c is the modified coupling conductance (in m^4 V^{-1} s^{-1}). Note that the capillaries are submitted to a gradient of water pressure in steady-state conditions and that generates, in turn, an electrical potential gradient.

Given the importance of the local electrical potential, ψ, in the above equations, we use the code proposed by *Leroy and Maineult* [2018] to solve the general Poisson-Boltzmann equation in each cylindrical pore at a given ionic concentration.

In the simulations, the ζ-potential depends on the ionic concentration in the bulk pore water and is determined by the following relationship [*Pride and Morgan*, 1991]:

$$\zeta(C^w) = a + b\log_{10}(C^w), \tag{28}$$

where a and b are fitting parameters. For this study we use the parameter values obtained by *Jaafar et al.* [2009] for NaCl brine: a=-6.43 mV and b=20.85 mV for silicate materials. Note that *Cherubini et al.* [2018] propose different values of a and b for carbonates based on experimental streaming potential measurements.

The electrical conductivity of the water also depends on the ionic concentration. In our simulation, we consider the *Sen and Goode* [1992] empirical model:

$$\sigma_w(C^w, T) = \left(a_1 + a_2 T + a_3 T^2\right) C^w - \left(\frac{a_4 + a_5 T}{1 - a_6\sqrt{C^w}}\right), \tag{29}$$

with $a_1 = 5.6$ S L m^{-1} mol^{-1}, $a_2 = 0.27$ S L m^{-1} mol^{-1} °C^{-1}, $a_3 = -1.51 \times 10^{-4}$ S L m^{-1} mol^{-1} °C^{-2}, $a_4 = 2.36$ (S L m^{-1} mol^{-1})$^{3/2}$, $a_5 = 0.099$ (S L m^{-1} mol^{-1} °C^{-1})$^{3/2}$, $a_6 = 0.214$ (mol^{-1})$^{-1/2}$, and in which the ionic concentration and the temperature are expressed in mol L^{-1} and °C, respectively.

3.2 2D pore network and related equation system

We consider a 2D pore network as shown in Fig. 2. At each node (i, j) of the grid, we applied *Kirchhoff* [1845]'s law for the conservation of the mass and of the electrical charge, which yields:

$$\begin{cases} -\gamma^h_{i-1,j\to i,j}(P_{i,j} - P_{i-1,j}) + \gamma^c_{i-1,j\to i,j}(V_{i,j} - V_{i-1,j}) \\ \qquad -\gamma^h_{i+1,j\to i,j}(P_{i,j} - P_{i+1,j}) + \gamma^c_{i+1,j\to i,j}(V_{i,j} - V_{i+1,j}) \\ \qquad -\gamma^h_{i,j-1\to i,j}(P_{i,j} - P_{i,j-1}) + \gamma^c_{i,j-1\to i,j}(V_{i,j} - V_{i,j-1}) \\ \qquad -\gamma^h_{i,j+1\to i,j}(P_{i,j} - P_{i,j+1}) + \gamma^c_{i,j+1\to i,j}(V_{i,j} - V_{i,j+1}) = 0 \\ \gamma^c_{i-1,j\to i,j}(P_{i,j} - P_{i-1,j}) - \gamma^e_{i-1,j\to i,j}(V_{i,j} - V_{i-1,j}) \\ \qquad \gamma^h_{i+1,j\to i,j}(P_{i,j} - P_{i+1,j}) - \gamma^e_{i+1,j\to i,j}(V_{i,j} - V_{i+1,j}) \\ \qquad \gamma^h_{i,j-1\to i,j}(P_{i,j} - P_{i,j-1}) - \gamma^e_{i,j-1\to i,j}(V_{i,j} - V_{i,j-1}) \\ \qquad \gamma^h_{i,j+1\to i,j}(P_{i,j} - P_{i,j+1}) - \gamma^e_{i,j+1\to i,j}(V_{i,j} - V_{i,j+1}) = 0 \end{cases} \tag{30}$$

where $\gamma_{x\to y}$ is the modified conductance of the tube linking node x to node y. With the appropriate boundary conditions (i.e., no fluxes over the lateral boundaries, no inflowing electrical flux at the upstream boundary and no outflowing electrical flux at the downstream boundary), we obtain a linear system whose unknowns are the $N_i \times N_j$ hydraulic pressure values at the nodes, the $N_i \times N_j$ electrical potential values at the nodes, the value of the electrical potential V_u in the upstream reservoir, and the value of the electrical potential V_d in the downstream reservoir. Note that all the tubes connecting two nodes have the same length l. See Appendix A for the full derivation of the system.

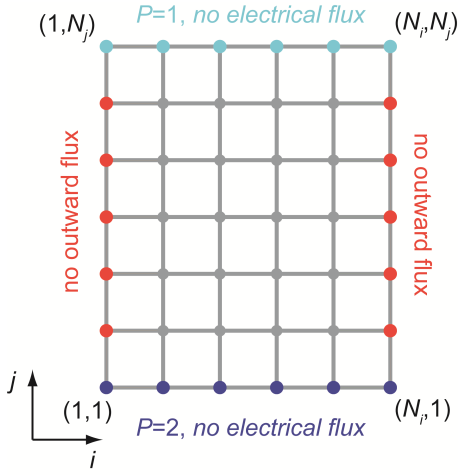

Figure 2. Scheme of the pore network organization and the boundary conditions used in our simulations. Note that all tubes have the same length l.

3.3 Pore size distribution

In this work, we investigate the effect of four different pore size distributions on streaming current generation: fractal, exponential symmetric, lognormal and double lognormal (i.e., bimodal). Note that we first built the networks for a pore size range between 1 and 100 μm (Fig. 3), then we shifted this range towards smaller pores in order to obtain smaller permeabilities while keeping constant the ratio $\alpha = R_{max}/R_{min}$. Hence, we obtained five different permeabilities for each pore size distribution.

3.3.1 Fractal distribution

We start with a fractal pore size distribution (Fig. 3a) as many geological porous media exhibit frequency distribution skewed towards smaller pore radii [*Dullien*, 2012]. It is also the pore size distribution used by *Guarracino and Jougnot* [2018] to develop their analytical model (i.e., Eq. 24).

The cumulative size distribution of pores whose radii are greater than or equal to R (m) is assumed to obey the following fractal law [*Tyler and Wheatcraft*, 1990; *Yu et al.*, 2003; *Guarracino et al.*, 2014]:

$$N(R) = \left(\frac{R_{REV}}{R}\right)^D, \tag{31}$$

where D is the fractal dimension of pore size with $1 < D < 2$ and $0 < R_{min} \leq R \leq R_{max} < R_{REV}$. Differentiating (31) with respect to R we obtain the number of pores whose radii are in the infinitesimal range R to $R + dR$:

$$dN = -DR_{REV}^D R^{-D-1} dR, \tag{32}$$

where the negative sign implies that the number of pores decreases with the increase of pore radius R. In fact, the resulting distribution is a decreasing exponential in a semilogarithmic space.

3.3.2 Exponential symmetric distribution

To generate the exponential symmetric distribution (Fig. 3b), we contracted the fractal distribution over one decade, we shifted it to the range 10-100 μm, then we added the symmetric part over the range 1-10 μm to obtain the exponentially increasing part, and finally we normalized the distribution to get a cumulative distribution comprised between 0 and 1.

3.3.3 Lognormal distribution

The lognormal distribution (Fig. 3c) is so that the decimal logarithm of the radius is normally distributed, as done in *Maineult et al.* [2017]. The probability P that $\log_{10}(R)$ is less than X is given by:

$$P(\log_{10}(R) \leq X) = \frac{1}{2} + \frac{1}{2} erf\left(\frac{X - \log_{10}(R_{peak})}{s\sqrt{2}}\right), \tag{33}$$

where R_{peak} is the value of the radius associated to the peak of the distribution, and s is the standard deviation.

3.3.4 Double lognormal distribution

The double lognormal distribution (Fig. 3d) is the sum of two lognormal distributions with the same standard deviation s, and writes :

$$P(\log_{10}(R) \leq X) = \frac{1}{2} + \frac{1}{4} erf\left(\frac{X - \log_{10}(R_{peak,1})}{s_1\sqrt{2}}\right) + \frac{1}{4} erf\left(\frac{X - \log_{10}(R_{peak,2})}{s_2\sqrt{2}}\right), \quad (34)$$

where the bimodal distribution is obtained through the choice of the two peaks for the distribution $R_{peak,1}$ and $R_{peak,2}$.

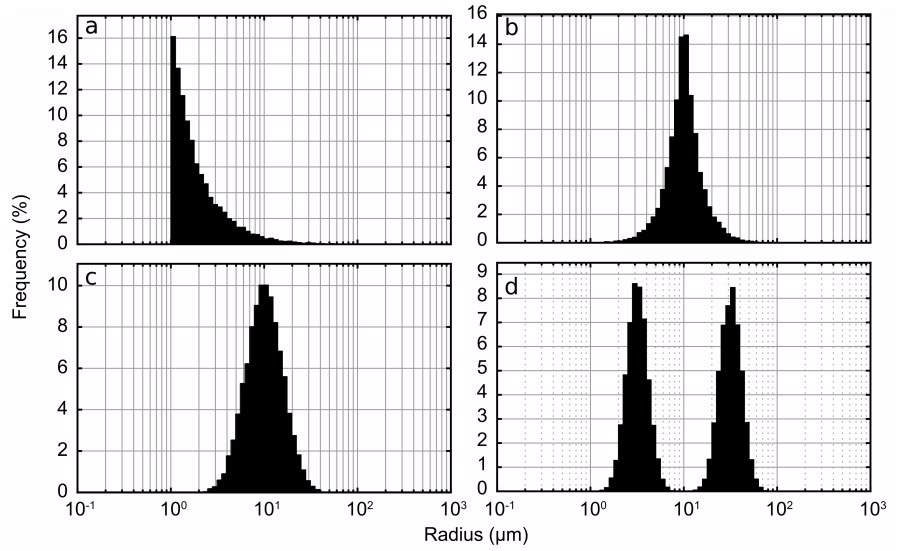

Figure 3. Pore size distributions used in this work: (a) fractal ($D = 1.5$), (b) exponential symmetric, (c) lognormal ($R_{peak} = 10\mu$m and $s = 0.45973$), and (d) double lognormal ($R_{peak,1} = 3.166\mu$m, $R_{peak,2} = 31.66\mu$m, and $s_1 = s_2 = s/2$). Note that the different permeabilities are obtained by shifting the distribution towards smaller pores but keeping constant the ratio $\alpha = R_{max}/R_{min}$.

3.4 Petrophysical parameters computation

In our numerical simulations, we impose a hydraulic pressure gradient and obtain the resulting voltage values V_u and V_d. It is then trivial to compute the corresponding electrokinetic coupling coefficient using,

$$C_{EK} = \frac{\Delta V}{\Delta P} = \frac{V_d - V_u}{P_{i,N_j} - P_{i,1}} = \frac{V_d - V_u}{2 - 1} = V_d - V_u. \quad (35)$$

Then, the effective excess charge density is obtained by modifying Eq. 3:

$$\hat{Q}_v = -\frac{\eta_w \sigma C_{EK}}{k}. \quad (36)$$

where the permeability is deduced from the pore network simulation. As we neglect the surface electrical conductivity, Eq. 36 can then be expressed by,

$$\hat{Q}_v = -\frac{\eta_w \sigma_w C_{EK}}{kF}. \tag{37}$$

where F is the formation factor, also deduced from the pore network simulation. Note that, as we neglect the surface conductivity of the medium, the formation factor is the ratio between the pore network and the pore water electrical conductivities: $F = \sigma_w/\sigma$. The computation of k/ϕ and $F\phi$ are described in Appendix B.

4 Numerical results

The simulations were run once for each given distribution (5 pore size distributions for each of the 4 types) and concentration (9 different concentrations) by solving the linear system described in the previous section; that is results for 180 pore networks with a size of 100×100. The results obtained from these simulations can be found in Appendix C. In our simulations, the temperature is fixed to 20°C. This section presents the simulation results on the effect of the pore size distributions on the two electrokinetic coupling parameters, C_{EK} and $\hat{Q}_v$, for a large range of permeabilities (from 10^{-16} to 10^{-10} m^2) and ionic concentrations (from 10^{-4} to 1 mol L^{-1}).

4.1 Influence of the pore size distribution on the permeability

The pore size distribution has a major impact on the pore network effective permeability. As one can see on Figs. 3 and 4, for a given range of capillary radius (i.e., from 1 to 100 μm), the fractal distribution contains a much higher number of thin capillaries than the exponential symmetric and the lognormal distributions. This yields a smaller effective permeability of the 2D pore network with fractal pore size distribution. By its bimodal nature, double lognormal networks (Figs. 3d) contain both larger and smaller pores than the exponential symmetric and lognormal networks (Figs. 3b and c). However, Fig. 4d shows that their random distribution yields that larger pores are isolated from each other by smaller pores, hence yielding a smaller effective permeability of the double lognormal networks.

Given the important similarity between the exponential symmetric and lognormal pore size distribution (Figs. 3b and c), it is not surprising that both networks have similar permeabilities.

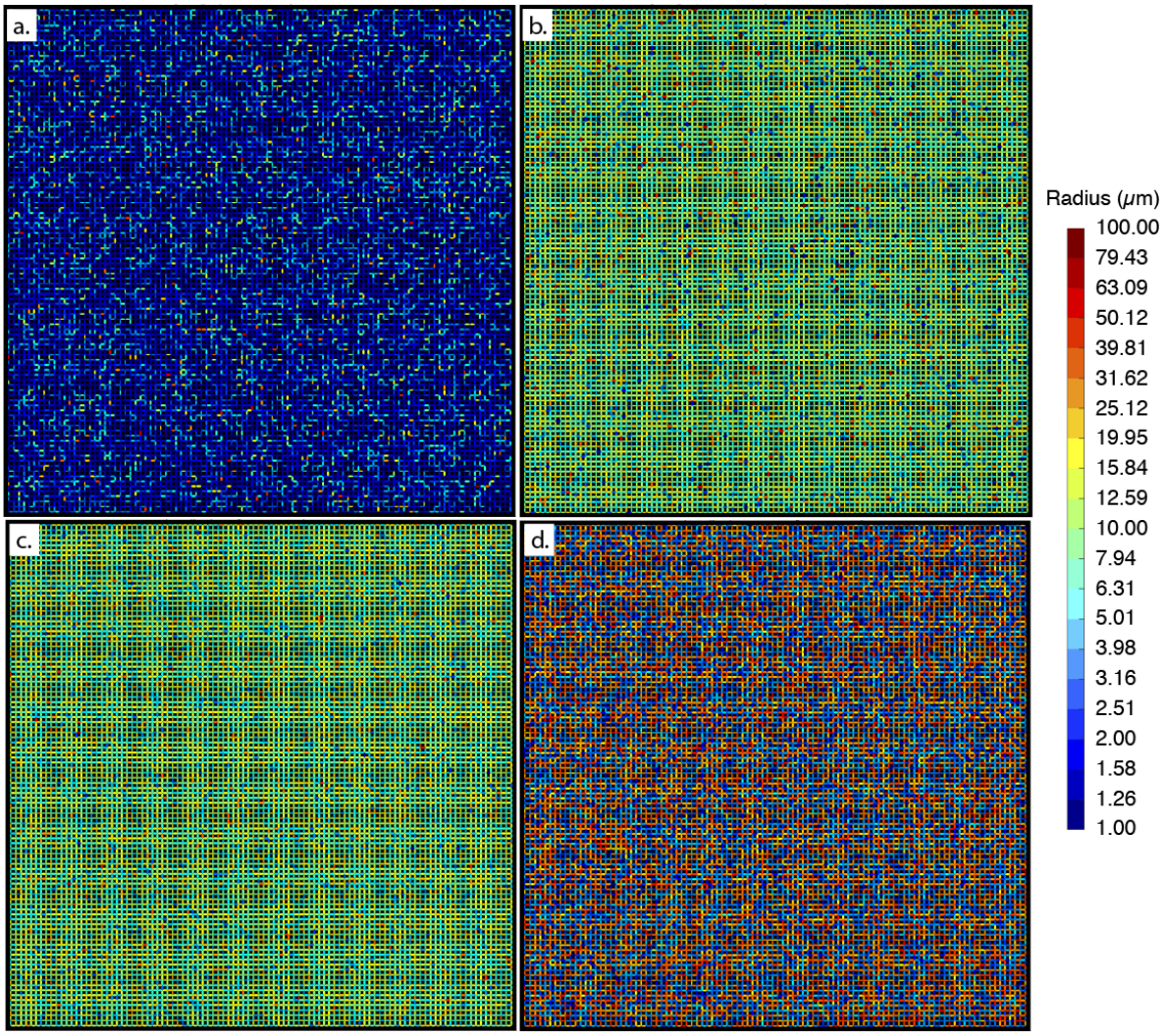

Figure 4. Examples of the pore networks used in this work: (a) fractal, (b) exponential symmetric, (c) lognormal, and (d) double lognormal (in these examples, the capillary sizes range from 1 to 100 μm). Note that the size of the networks was 100 $\times$ 100 nodes. See the corresponding frequency pore size distributions in Fig. 3.

The Johnson's length [*Schwartz et al.*, 1989], Λ (m), is a petrophysical parameter that has been shown to be representative of a medium permeability. *Revil and Cathles* [1999] proposes a simple model to predict the medium permeability:

$$k = \frac{\Lambda^2}{8F}. \tag{38}$$

Figures 5a and b compare the permeability resulting from the pore network simulations and the ones predicted by the model of *Revil and Cathles* [1999] (Eq. 38) using the hydraulic (Λ_h) and electrical (Λ_e) Johnson's lengths deduced from the pore network sim-

ulations [see *Bernabé and Revil*, 1995, and Appendix B], respectively. One can see that the model from *Revil and Cathles* [1999] tends to overpredict the effective permeabilities of the networks, except for the double lognormal network permeabilities predicted by Λ_h. Nevertheless, both predictions are rather good (within half an order of magnitude), showing the interest of Eq. (38) to characterize a porous medium [see also the discussions in *Maineult et al.*, 2018].

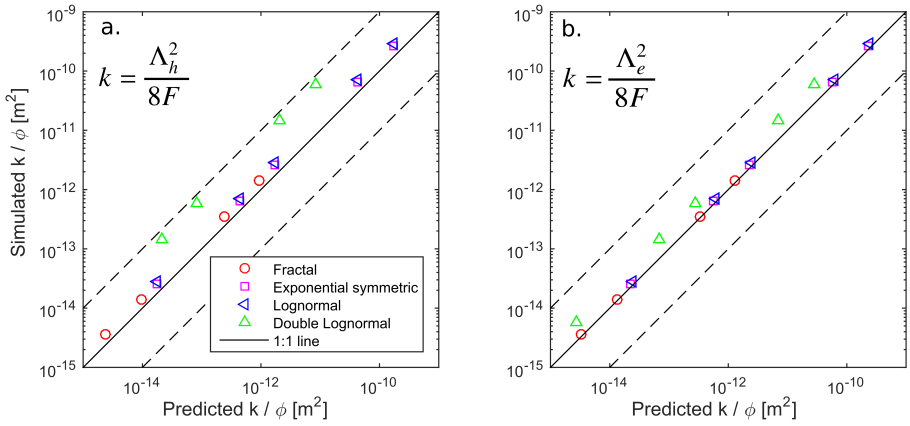

Figure 5. Comparison between the simulated permeabilities (normalized by the porosities) with the pore network model and the ones predicted by the model of *Revil and Cathles* [1999] based on the (a) hydraulic, Λ_h, and (b) electrical, Λ_e, Johnson's lengths, respectively (see definitions in Appendix B). The solid black line corresponds to the 1:1 line, while the dashed lines correspond to the one order of magnitude range.

4.2 Evolution of the coupling parameters with the ionic concentration and permeability

Figure 6a presents the evolution of the coupling coefficient as a function of the pore water ionic concentration. The simulation results clearly indicate that the NaCl ionic concentration drives the amplitude of the coupling coefficient, while the influence of pore size distribution is rather small (from less than 1% for 1 mol L^{-1} up to 66% for 10^{-4} mol L^{-1}). This is consistent with the Helmholtz-Smoluchowski equation (Eq. 2) that contains

two parameters which are concentration dependent, the ζ-potential (Eq. 28) and the pore water electrical conductivity (Eq. 29), but none related to the medium geometrical properties.

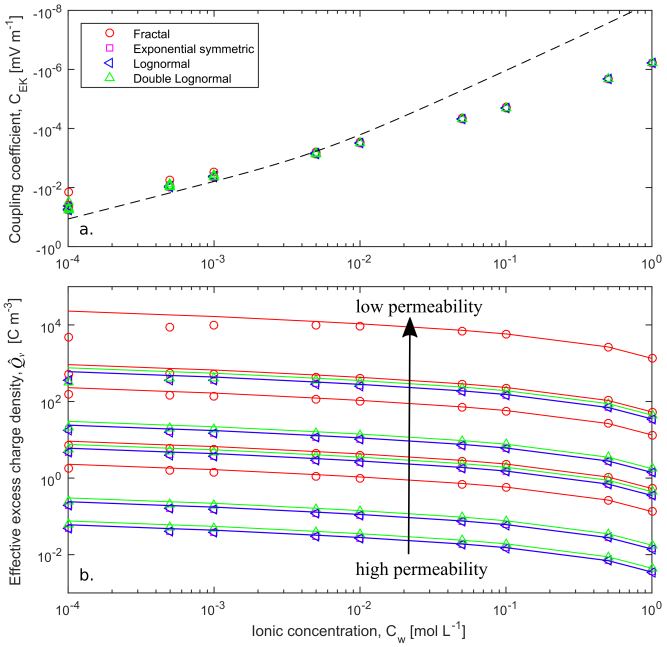

Figure 6. Simulation results presented as (a) electrokinetic coupling coefficient and (b) effective excess charge density as a function of the ionic concentrations for the different pore size distributions. In the (a) subplot, the dashed black line corresponds to the empirical relationship proposed by *Linde et al.* [2007] (Eq. 39). In the (b) subplot, the solid lines in colors correspond to the model predictions of *Guarracino and Jougnot* [2018] (Eq. 24).

Linde et al. [2007] proposed an empirical model depending only on the pore water ionic concentation (through its electrical conductivity) based on a large data set of coupling coefficients:

$$\log |C_{EK}| = b_1 + b_2 \log(\sigma_w) + b_3 \log(\sigma_w)^2, \tag{39}$$

where b_1 = -0.895, b_2 = -1.319, and b_3 = -0.1227. Fig. 6a shows that this empirical model matches rather well for ionic concentrations between 10^{-4} to 10^{-2} mol L^{-1}, clearly confirming that ionic concentration is the main driver.

Figures 7a and b show that the variation of C_{EK} as a function of the network permeability (hence of the network pore size distribution, see previous subsection) strongly

depends on the ionic concentration. Indeed, C_{EK} diminishes importantly when permeability increases at low salinity ($C^w_{NaCl} = 10^{-4}$ mol L^{-1} in Fig. 7a), but it barely varies for higher salinity ($C^w_{NaCl} = 1$ mol L^{-1} in Fig. 7b). As for the permeabilities, C_{EK} for the exponential symmetric and lognormal networks are very similar, while the fractal distribution has a very different behaviour, probably related to the larger number of smaller pores.

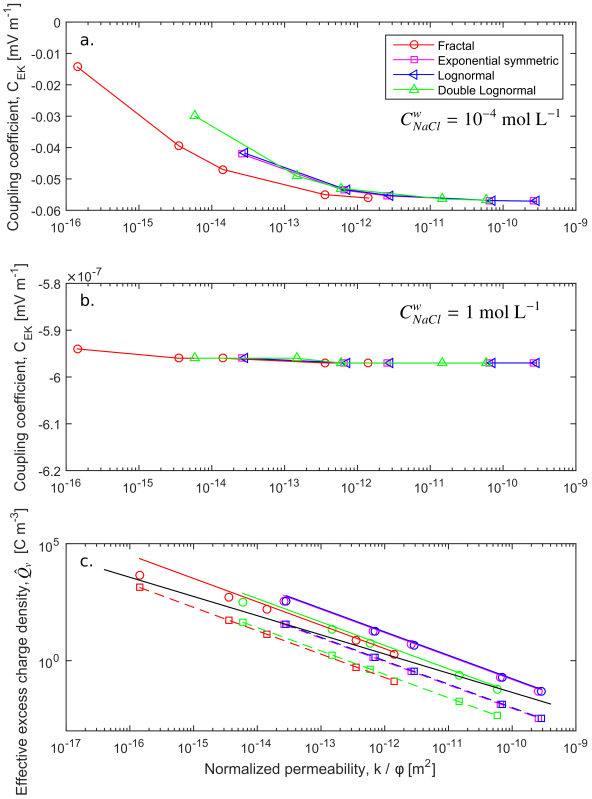

Figure 7. Electrokinetic coupling coefficient as a function of the permeability normalized by the porosity for (a) $C_w = 10^{-4}$ mol L^{-1} and (b) $C_w = 1$ mol L^{-1} from our numerical simulation. (c) Effective excess charge density as a function of the permeability normalized by the porosity for the different pore size distributions for $C_w = 10^{-4}$ and 1 mol L^{-1}. Note that each point corresponds to the simulation result for a given network. On the (c) subplot, the solid and dashed colored lines correspond to the model predictions of *Guarracino and Jougnot* [2018] (Eq. 24) for $C_w = 10^{-4}$ mol L^{-1} and $C_w = 1$ mol L^{-1}, respectively; while the single black solid line is the prediction from *Jardani et al.* [2007] with a fixed porosity $\phi = 0.4$.

Contrarily to the electrokinetic coupling coefficient, the effective excess charge density computed from Eq. (37) strongly depends both on ionic concentration and network

permeability. Figures 6b and 7c show that the permeability is the most important parameter controlling the magnitude of $\hat{Q}_v$: a decrease of 4 orders of magnitude in permeability yields an increase of 4 orders of magnitude for $\hat{Q}_v$. This behaviour is consistent with experimental data and models from the literature [e.g., *Titov et al.*, 2002; *Jardani et al.*, 2007; *Jougnot et al.*, 2012]. The influence of the ionic concentration on the effective excess charge density is also consistent with experimental data from the litterature: an increase of 4 orders of magnitude in the ionic concentration yields a decrease of around 1 order of magnitude for $\hat{Q}_v$ [e.g., *Pengra et al.*, 1999; *Jougnot et al.*, 2015; *Cherubini et al.*, 2018].

4.3 Testing the model of *Guarracino and Jougnot* [2018]

The dependence of the effective excess charge on both the permeability and the pore water ionic concentration is discussed in details in *Guarracino and Jougnot* [2018] and taken into account in their model (Eq. 24). Figures 6b and 7c show the very good agreement between the $\hat{Q}_v$ obtained from the network simulations and the one predicted by the *Guarracino and Jougnot* [2018]'s model as a function of the ionic concentration and permeability, respectively. All the parameters needed for the model (Eq. 24) are either input parameters (C^w, thus ζ and l_D, from Eqs. 28 and 18, respectively) or calculated outputs from the simulations (k/ϕ, from Eq. 63). Following the proposition of *Guarracino and Jougnot* [2018], we use the *Winsauer et al.* [1952] model to determine the hydraulic tortuosity from:

$$\tau = \sqrt{F\phi}. \tag{40}$$

Therefore, none of the parameters were fitted in order to obtain these predictions in very good agreement with the computations from our numerical simulations. Note that the *Jardani et al.* [2007]'s model corresponds fairly well to an average trend, regardless the network and the ionic concentration.

Figure 8 represents the same data (i.e., for all networks and ionic concentrations) along a 1:1 line. One can notice that the model slightly overpredicts the numerical effective excess charge for very high $\hat{Q}_v$, that is for low permeability and low ionic concentration. This can be explained by the model limitation: the capillary radius has to be significantly larger than the Debye length $R \gg 5l_D$.

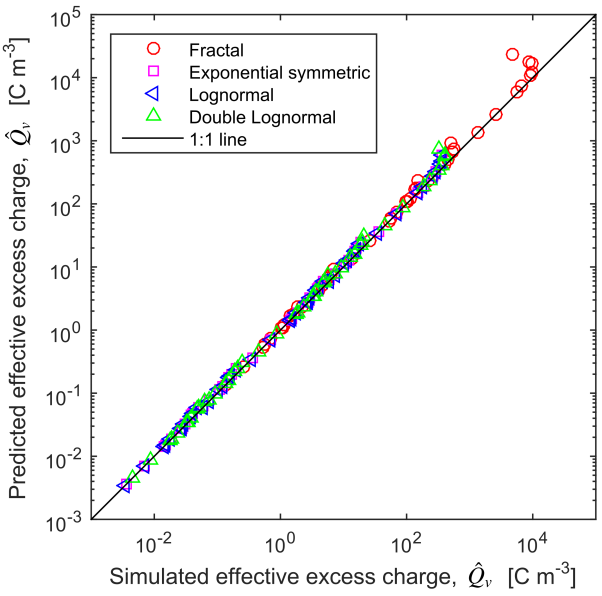

Figure 8. Comparison between the simulated effective excess charge density with the pore network model and the one predicted by the analytical model of *Guarracino and Jougnot* [2018]. The solid black line corresponds to the 1:1 line.

4.4 Limitation of the model *Guarracino and Jougnot* [2018] in small pores at low ionic concentration

In this subsection, we investigate why the largest misfits are obtained for the highest values of effective excess charge, that is, for the lowest ionic concentrations (i.e., thickest diffuse layers) and for the lowest permeabilities (i.e., smallest pore sizes). In Fig. 8, one can see that it is especially the case for the fractal distribution, where the amount of small pores is larger than in the other distributions (see Fig. 3).

Therefore, we consider the smallest investigated capillaries ($R = 0.1\mu$m) filled by a pore water containing the lowest ionic concentration of NaCl, $C^w_{NaCl} = 10^{-4}$ mol L^{-1} (i.e., $l_D = 3.04 \times 10^{-8}$ m, hence $R = 3.29 l_D < 4 l_D$), i.e., the most extreme case for the present study. Then, we use the numerical code of *Leroy and Maineult* [2018] to solve for the Poisson-Boltzmann equation in an infinite charged cylinder and the ζ-potential is $\zeta = -89.8$ mV following *Jaafar et al.* [2009] (Eq. 28). Figures 9 and 10 illustrate the limitation of the Debye-Hückel approximation used by *Guarracino and Jougnot* [2018]

by comparing its results to the Poisson-Boltzmann numerical resolution using *Leroy and Maineult* [2018].

Figure 9a compares the local electrical potential calculated with the Debye-Hückel approximation (Eq. 17) and the general Poisson-Boltzmann (Eq. 12), while Figure 9b displays the corresponding residual potential. Given that $R < 4l_D$, one can see that $\psi \neq 0$ mV in the middle of the pore, this implies that the EDL overlap [e.g., *Gonçalvès et al.*, 2007]. The effect on the local electrical potential is substantial: the residual is close to 50% at the center of the pore. This has a significant effect on the distribution of the ions as shown in Figs. 9c and d. For $R = 0.1\mu$m and $C^w_{NaCl} = 10^{-4}$ mol L^{-1}, one can see that there is no free electrolyte, therefore the local ionic concentrations are different from the bulk water concentrations $C_{Na} \gg C^w_{Na}$ and $C_{Cl} \ll C^w_{Cl}$ in the entire capillary. Consequently, the distribution of the excess charge density $\bar{Q}_v$ calculated from Eq. 19 in a small capillary for low concentrations is strongly affected by the Debye-Hückel approximation (Fig. 10b and c). This example on the most extreme case used in the previous simulation clearly demonstrates why the model of *Guarracino and Jougnot* [2018] cannot correctly predict the effective excess charge density in pores such as $R < 5l_D$, that is when the thin double layer assumption is not respected.

5 Discussion and conclusion

In the present paper, we present numerical simulations of streaming current generation in water saturated 2D pore networks with different pore size distributions, hence different permeabilities (from 10^{-16} to 10^{-10} m^2). We performed the simulations to obtain the electrokinetic coupling coefficients for pore water having a NaCl concentrations ranging from 10^{-4} to 1 mol L^{-1}. From these simulations we deduced the effective excess charge density from the corresponding coupling coefficient and performed a detailed analysis of the behaviour of these two electrokinetic coupling parameters.

Our first finding is that the pore size distribution has a primary influence on the medium's permeability (Fig. 5) as expected from the literature, but almost no influence on the electrokinetic coupling coefficient (Figs. 6a and 7b). This is consistent with the widely used model of Helmholtz-Smoluchowski (Eq. 2) which does not include any information nor parameters about the medium's texture and has been proven to be useful in a large range of natural geological media (as long as the surface conductivity can be ne-

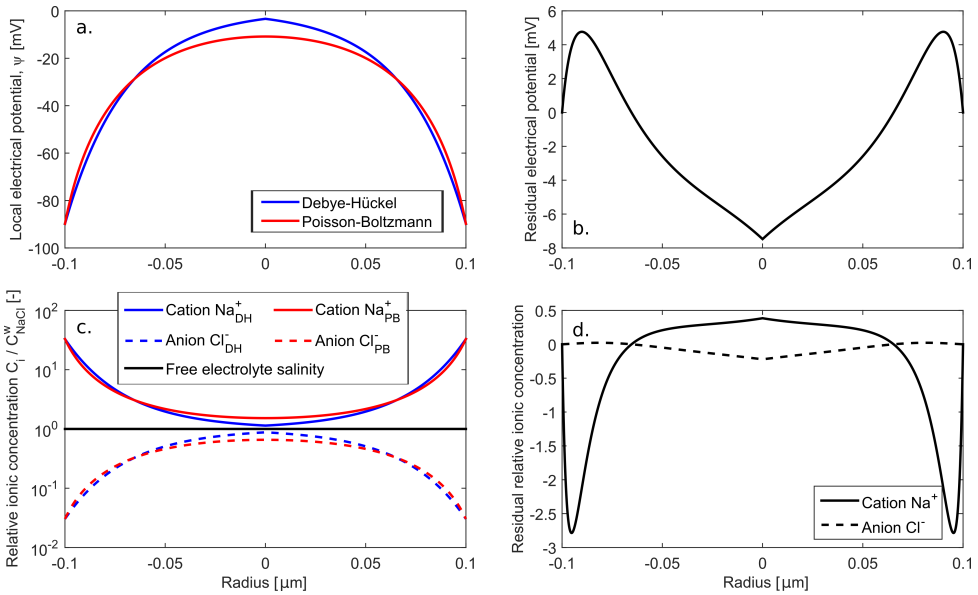

Figure 9. Comparison between the Debye-Hückel approximation and the Poisson-Boltzmann equation to compute (a) the electrical potential distribution and (c) the ionic species relative concentration distribution in a small capillary ($R = 10^{-7}$ m) containing a NaCl electrolyte with $C^w_{NaCl} = 10^{-4}$ mol L^{-1} (i.e., $l_D = 3.04 \times 10^{-8}$ m). (b) and (d) show the corresponding residual electrical potential and relative ionic concentration, respectively. Note that the x-axis is a modified coordinate $r' = R - r$ such as $r' = 0$ m in the middle of the capillary.

glected). It is therefore clear that the pore water chemistry is the main driver for the C_{EK} as proposed by the empirical model of *Linde et al.* [2007].

On the contrary, the pore size distribution has a strong influence on the effective excess charge density through the permeability, as it was expected from both empirical [e.g., *Titov et al.*, 2002; *Jardani et al.*, 2007; *Cherubini et al.*, 2018] and theoretical evidence [e.g., *Jougnot et al.*, 2012; *Guarracino and Jougnot*, 2018]. When considering Eq. 3 and Eq. 24 [*Guarracino and Jougnot*, 2018], it is clear that the permeability simplifies out in the electrokinetic coupling coefficient C_{EK}. One can also note that the analytical model of *Guarracino and Jougnot* [2018], originally defined for fractal media, performs well for any kind of pore size distribution (even double porosity ones) given that this information is included in the model through the medium's permeability and porosity that appear explicitely.

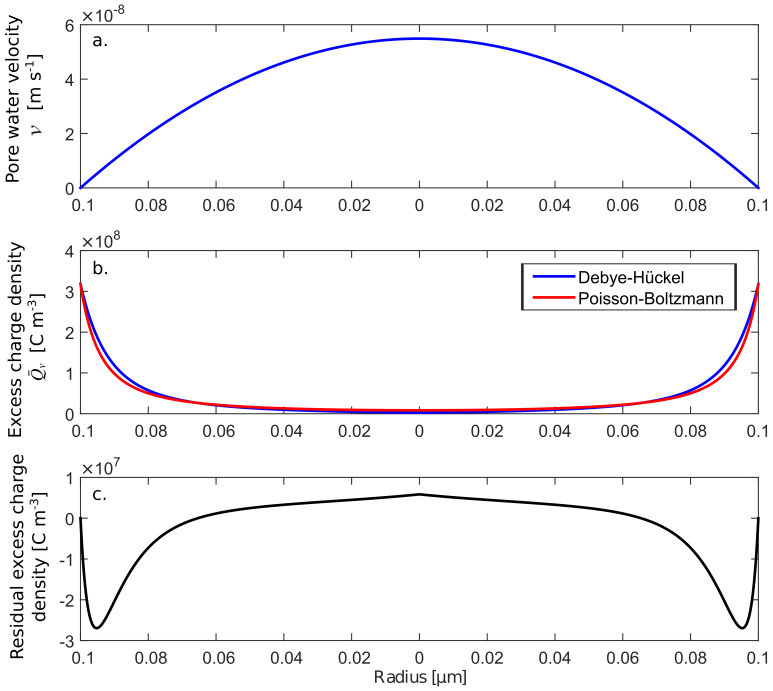

Figure 10. (a) Distribution of the pore water velocity in a small capillary ($R = 10^{-7}$ m) following Poiseuille's law. (b) Comparison of the excess charge density distribution obtained from the Debye-Hückel approximation and the numerical Poisson-Boltzmann resolution in the same capillary ($R = 10^{-7}$ m) containing a NaCl electrolyte with $C^w_{NaCl} = 10^{-4}$ mol L^{-1} (i.e., $l_D = 3.04 \times 10^{-8}$m), and (c) the corresponding residual. Note that the x-axis is a modified coordinate $r' = R - r$ such as $r' = 0$ m in the middle of the capillary.

Nevertheless, the observations from the previous paragraphs are not valid for very small pores filled by pore water with a low ionic concentration, that is $C^w < 10^{-3}$ mol L^{-1} (Figs. 6a and 7a). Indeed, when the salinity decreases and if the medium has small pores (Fig. 7a), C_{EK} becomes highly dependent on the permeability. This behaviour is consistent with the previous work of *Bernabé* [1998] on pore networks, but also with the experimental results of *Jouniaux and Pozzi* [1995b] (using a very resistive water). This effect is directly related to the EDL in the pore space: when l_D becomes important in comparison to the pore radius ($R < 4l_D$), the diffuse layers from both sides of the capillary start to overlap, yielding a strong effect on the amount of excess charge that can be dragged by the water flow (e.g. Figs. 9 and 10). Such effect also impacts the performance of the model

of *Guarracino and Jougnot* [2018] to reproduce the simulated effective excess charge densities (Fig. 8).

In geological media and under most environmental conditions (i.e. groundwater for human consumption or subsurface reservoirs), 10^{-4} mol L^{-1} represents an extreme case scenario [e.g., *McCleskey*, 2011]. Indeed, ionic strengths (i.e., a proxy for ionic concentration) in potable water typically vary between 10^{-3} and 10^{-2} mol L^{-1}, while reservoirs can be saturated with brines having much higher ionic concentrations depending on the formation. Therefore, the assumption of $R \gg 4l_D$ can be considered valid in most natural systems, which allows the use of the model recently proposed by *Guarracino and Jougnot* [2018] (valid for $R > 5l_D$).

In addition to the intrinsic limitation of the model proposed by *Guarracino and Jougnot* [2018], the fact that we neglect the surface conductivity in Eq. 37 even for the lowest ionic concentration and smaller pores can also contribute to the misfit. Further developments of the present 2D pore network code should also include an explicit calculation of the surface conductivity for the determination of the effective excess charge density. This would open the possibility of studying the behaviour of micro-porous media such as clay rocks. Additional improvements on our pore network modeling approach could also allow further studies, among which: relating pore lengths to pore sizes to mimic more natural observations (e.g., small pore sizes are usually related to small pore length), considering connectivities higher than 4 for each nodes. Nevertheless, despite all these limitations, the two approaches that we consider here converge towards similar predictions, and this is remarkable, since they are totally independent. Further works will require the overcoming of these limitations, and also to implement 3D network, in order to produce synthetic media closer to real ones. A more advance approach would be extracting pore networks that replicates the pore space obtain from rock sample imagery [e.g., *Bryant and Blunt*, 1992] to solve for the electrokinetic coupling.

We believe that the present study will help to better understand the theoretical links between the electrokinetic coupling coefficient and the effective excess charge approaches, providing a mechanistic study of the streaming potential generation under water saturated conditions. In the future, we will try to extend this approach and the corresponding study for partially saturated conditions [see *Jougnot et al.*, 2012; *Soldi et al.*, 2019].

Appendix A: Pressure and electrical potential equations in the pore network

Inside the network, that is for the indexes $(i, j) \in [2, N_i - 1] \times [2, N_j - 1]$, Eq. 30 is rewritten as,

$$\begin{cases} \gamma^h_{i-1,j\to i,j} P_{i-1,j} + \gamma^h_{i+1,j\to i,j} P_{i+1,j} - \kappa^h_{i,j} P_{i,j} + \gamma^h_{i,j-1\to i,j} P_{i,j-1} + \gamma^h_{i,j+1\to i,j} P_{i,j+1} \\ \qquad -\gamma^c_{i-1,j\to i,j} V_{i-1,j} - \gamma^c_{i+1,j\to i,j} V_{i+1,j} + \kappa^c_{i,j} V_{i,j} - \gamma^c_{i,j-1\to i,j} V_{i,j-1} - \gamma^c_{i,j+1\to i,j} V_{i,j+1} = 0 \\ -\gamma^c_{i-1,j\to i,j} P_{i-1,j} - \gamma^c_{i+1,j\to i,j} P_{i+1,j} + \kappa^c_{i,j} P_{i,j} - \gamma^c_{i,j-1\to i,j} P_{i,j-1} - \gamma^c_{i,j+1\to i,j} P_{i,j+1} \\ \qquad +\gamma^e_{i-1,j\to i,j} V_{i-1,j} + \gamma^e_{i+1,j\to i,j} V_{i+1,j} - \kappa^e_{i,j} V_{i,j} + \gamma^e_{i,j-1\to i,j} V_{i,j-1} + \gamma^e_{i,j+1\to i,j} V_{i,j+1} = 0 \end{cases} \tag{41}$$

with,

$$\begin{cases} \kappa^h_{i,j} = \left(\gamma^h_{i-1,j\to i,j} + \gamma^h_{i+1,j\to i,j} + \gamma^h_{i,j-1\to i,j} + \gamma^h_{i,j+1\to i,j}\right) \\ \kappa^c_{i,j} = \left(\gamma^c_{i-1,j\to i,j} + \gamma^c_{i+1,j\to i,j} + \gamma^c_{i,j-1\to i,j} + \gamma^c_{i,j+1\to i,j}\right) \\ \kappa^e_{i,j} = \left(\gamma^e_{i-1,j\to i,j} + \gamma^e_{i+1,j\to i,j} + \gamma^e_{i,j-1\to i,j} + \gamma^e_{i,j+1\to i,j}\right) \end{cases} \tag{42}$$

in $i = 1$ (no outward current) and $j \in [2, N_j - 1]$, we have

$$\begin{cases} \gamma^h_{2,j\to 1,j} P_{2,j} - \kappa^h_{1,j} P_{1,j} + \gamma^h_{1,j-1\to 1,j} P_{1,j-1} + \gamma^h_{1,j+1\to 1,j} P_{1,j+1} \\ \qquad -\gamma^c_{2,j\to 1,j} V_{2,j} + \kappa^c_{1,j} V_{1,j} - \gamma^c_{1,j-1\to 1,j} V_{1,j-1} + \gamma^c_{1,j+1\to 1,j} V_{1,j+1} = 0 \\ -\gamma^c_{2,j\to 1,j} P_{2,j} + \kappa^c_{1,j} P_{1,j} - \gamma^c_{1,j-1\to 1,j} P_{1,j-1} - \gamma^c_{1,j+1\to 1,j} P_{1,j+1} \\ \qquad +\gamma^e_{2,j\to 1,j} V_{2,j} - \kappa^e_{1,j} V_{1,j} - \gamma^e_{1,j-1\to 1,j} V_{1,j-1} + \gamma^e_{1,j+1\to 1,j} V_{1,j+1} = 0 \end{cases} \tag{43}$$

with

$$\begin{cases} \kappa^h_{1,j} = \left(\gamma^h_{2,j\to 1,j} + \gamma^h_{1,j-1\to 1,j} + \gamma^h_{1,j+1\to 1,j}\right) \\ \kappa^c_{1,j} = \left(\gamma^c_{2,j\to 1,j} + \gamma^c_{1,j-1\to 1,j} + \gamma^c_{1,j+1\to 1,j}\right) \\ \kappa^e_{1,j} = \left(\gamma^e_{2,j\to 1,j} + \gamma^e_{1,j-1\to 1,j} + \gamma^e_{1,j+1\to 1,j}\right) \end{cases} \tag{44}$$

in $i = N_i$ (no outward current) and $j \in [2, N_j - 1]$, we have

$$\begin{cases} \gamma^h_{N_i-1,j\to N_i,j} P_{N_i-1,j} - \kappa^h_{N_i,j} P_{N_i,j} + \gamma^h_{N_i,j-1\to N_i,j} P_{N_i,j-1} + \gamma^h_{N_i,j+1\to N_i,j} P_{N_i,j+1} \\ \qquad -\gamma^c_{N_i-1,j\to N_i,j} V_{N_i-1,j} + \kappa^c_{N_i,j} V_{N_i,j} - \gamma^c_{N_i,j-1\to N_i,j} V_{N_i,j-1} + \gamma^c_{N_i,j+1\to N_i,j} V_{N_i,j+1} = 0 \\ -\gamma^c_{N_i-1,j\to N_i,j} P_{N_i-1,j} + \kappa^c_{N_i,j} P_{N_i,j} - \gamma^c_{N_i,j-1\to N_i,j} P_{N_i,j-1} - \gamma^c_{N_i,j+1\to N_i,j} P_{N_i,j+1} \\ \qquad +\gamma^e_{N_i-1,j\to N_i,j} V_{N_i-1,j} - \kappa^e_{N_i,j} V_{N_i,j} - \gamma^e_{N_i,j-1\to N_i,j} V_{N_i,j-1} + \gamma^e_{N_i,j+1\to N_i,j} V_{N_i,j+1} = 0 \end{cases} \tag{45}$$

with

$$\left\{\begin{array}{l} \kappa^h_{N_i,j} = \left(\gamma^h_{N_i-1,j\to N_i,j} + \gamma^h_{N_i,j-1\to N_i,j} + \gamma^h_{N_i,j+1\to N_i,j}\right) \\ \kappa^c_{N_i,j} = \left(\gamma^c_{N_i-1,j\to N_i,j} + \gamma^c_{N_i,j-1\to N_i,j} + \gamma^c_{N_i,j+1\to N_i,j}\right) \\ \kappa^e_{N_i,j} = \left(\gamma^e_{N_i-1,j\to N_i,j} + \gamma^e_{N_i-1,j-1\to N_i-1,j} + \gamma^e_{N_i-1,j+1\to N_i-1,j}\right) \end{array}\right. . \tag{46}$$

In $j = 1$, the following conditions are imposed for the hydraulic pressure and electrical potential:

$$\left\{\begin{array}{l} P_{i,1} = 2 \\ V_{i,1} = V_u \end{array}\right. , \tag{47}$$

There is no inflowing electrical current, that is:

$$\sum_{i=1}^{N_i} J_{i,1\to i,2} l = \sum_{i=1}^{N_i} \left(\gamma^c_{i,1\to i,2}\left(P_{i,2} - P_{i,1}\right) - \gamma^e_{i,1\to i,2}\left(V_{i,2} - V_{i,1}\right)\right) = 0, \tag{48}$$

which yields:

$$-\sum_{i=1}^{N_i} \gamma^c_{i,1\to i,2} P_{i,1} + \left(\sum_{i=1}^{N_i} \gamma^e_{i,1\to i,2}\right) V_u + \sum_{i=1}^{N_i} \gamma^c_{i,1\to i,2} P_{i,2} - \sum_{i=1}^{N_i} \gamma^e_{i,1\to i,2} V_{i,2} = 0. \tag{49}$$

Finally, in $j = N_j$, the conditions are:

$$\left\{\begin{array}{l} P_{i,N_j} = 1 \\ V_{i,N_j} = V_d \end{array}\right. , \tag{50}$$

There is no outflowing electrical current, that is:

$$\sum_{i=1}^{N_i} J_{i,N_j-1\to i,N_j} l = \sum_{i=1}^{N_i} \left(\gamma^c_{i,N_j-1\to i,N_j}\left(P_{i,N_j} - P_{i,N_j-1}\right) - \gamma^e_{i,N_j-1\to i,N_j}\left(V_{i,N_j} - V_{i,N_j-1}\right)\right) = 0, \tag{51}$$

which yields:

$$-\sum_{i=1}^{N_i} \gamma^c_{i,N_j-1\to i,N_j} P_{i,N_j-1} + \left(\sum_{i=1}^{N_i} \gamma^e_{i,N_j-1\to i,N_j}\right) V_{i,N_j-1} + \sum_{i=1}^{N_i} \gamma^c_{i,N_j-1\to i,N_j} P_{i,N_j} - \sum_{i=1}^{N_i} \gamma^e_{i,N_j-1\to i,N_j} V_d = 0. \tag{52}$$

The set of equations described above (Eqs. 41-47, 49-50, 52) forms a linear system. The unknowns are the hydraulic pressure, $P_{i,j}$, and the electrical potential, $V_{i,j}$, at all nodes and the two boundary electrical potentials V_u and V_d.

Appendix B: Numerical determination of the pore network permeability, formation factor, and Johnson's lengths

For a laminar flow, i.e. following Poiseuille's law, the hydraulic flux $F_{x\to y}$ through a capillary linking two nodes x and y writes:

$$F_{x\to y} = \frac{\pi R_{x\to y}^4}{8\eta_w}\frac{P_x - P_y}{l} = g_{x\to y}^h\left(P_x - P_y\right). \tag{53}$$

The length of the capillary, l, is eliminated by introducing a modified hydraulic flux defined as:

$$\Phi_{x\to y}^h = F_{x\to y}l = \frac{\pi R_{x\to y}^4}{8\eta_w}\left(P_x - P_y\right) = \gamma_{x\to y}^h\left(P_x - P_y\right). \tag{54}$$

Neglecting the surface electrical conductivity, the electrical flux $J_{x\to y}$ corresponds to:

$$J_{x\to y} = \sigma_w \pi R_{x\to y}^2\frac{V_x - V_y}{l} = g_{x\to y}^e\left(V_x - V_y\right). \tag{55}$$

The length of the capillary, l, is eliminated by introducing a modified electrical flux defined as:

$$\Phi_{x\to y}^e = \frac{J_{x\to y}l}{\sigma_w} = \pi R_{x\to y}^2\left(V_x - V_y\right) = \gamma_{x\to y}^e\left(V_x - V_y\right). \tag{56}$$

At any node in the square network, *Kirchhoff* [1845]'s law yields

$$Z_{i,j-1\to i,j} + Z_{i-1,j\to i,j} + Z_{i+1,j\to i,j} + Z_{i,j+1\to i,j} = 0. \tag{57}$$

with Z standing for F or J, respectively. Eq. 53 or 55, leads to

$$\begin{aligned} a_{i,j-1\to i,j}X_{i,j-1} + a_{i-1,j\to i,j}X_{i-1,j} - \left(a_{i,j-1\to i,j} + a_{i-1,j\to i,j} + a_{i+1,i\to i,j} + a_{i,j+1\to i,j}\right) \\ + a_{i+1,j\to i,j}X_{i+1,j} + a_{i,j+1\to i,j}X_{i,j+1} = 0. \end{aligned} \tag{58}$$

with $a = R^4$ and $X = P$ or $a = R^2$ and $X = V$ for the hydraulic or the electrical case, respectively.

For the nodes at the border of the network, Eq. 58 is easily modified to take into account the boundary conditions (i.e., no outward flow for $i = 1$ and $i = N_i$, $P = 1$ or $V = 1$ for $j = 1$, and $P = 0$ or $V = 0$ for $j = N_j$).

A linear system is obtained; the N_iN_j unknowns are the hydraulic pressure or electrical potential at the nodes of the network. Once the system is solved, the modified fluxes can be computed using Eqs. 54 or 56.

The effective permeability of the pore network k (m^2) is then computed using Darcy's law:

$$k = \frac{\eta_w QL}{S \mid \Delta P \mid} = \frac{\eta_w}{l^2}\frac{N_j - 1}{N_i - 1}\frac{\Phi_{\sum out/in}^h}{\mid \Delta P \mid}, \tag{59}$$

where Q is the hydraulic flux, L the length of the network along the flux direction (i.e., the j-direction), S the transversal section, and the total out-flowing and in-flowing fluxes are given by:

$$\begin{cases} \Phi^h_{\sum out} = \sum_{i=1}^{N_i-1} \Phi^h_{i,N_j-1\rightarrow i,N_j} \\ \Phi^h_{\sum in} = \sum_{i=1}^{N_i-1} \Phi^h_{i,1\rightarrow i,2} \end{cases} \tag{60}$$

In order to estimate the section and porosity of the network, we extend the 2D network into a virtual 3D one by adding two vertical capillaries of length $l/2$ at each node, but not contributing to the transport. This yields:

$$S = (N_i - 1)\, l^2 \tag{61}$$

$$\phi = \frac{\left((N_i - 1)\, N_j + \left(N_j - 1\right) N_i + N_i N_j\right) \pi \langle R^2 \rangle l}{(N_i - 1)\left(N_j - 1\right) l^3} \tag{62}$$

Extracting l^2 from Eq. 62 and given that $\mid \Delta P \mid = 1$, the effective permeability can be determined by:

$$\frac{k}{\phi} = \frac{\eta_w}{\pi \langle R^2 \rangle} \frac{\left(N_j - 1\right)^2}{(N_i - 1)\, N_j + \left(N_j - 1\right) N_i + N_i N_j} \Phi^h_{\sum out/in}. \tag{63}$$

Given that the surface conductivity can be neglected, the formation factor F of the network can be computed by:

$$\frac{1}{F} = \frac{\sigma}{\sigma_w} = \frac{1}{\sigma_w} \frac{JL}{S \mid \Delta V \mid} = \frac{1}{l^2} \frac{N_j - 1}{N_i - 1} \frac{\Phi^e_{\sum out/in}}{\mid \Delta V \mid}. \tag{64}$$

Then, considering that $\mid \Delta V \mid = 1$, the formation factor is then defined by:

$$\frac{1}{F\phi} = \frac{1}{\pi \langle R^2 \rangle} \frac{\left(N_j - 1\right)^2}{(N_i - 1)\, N_j + \left(N_j - 1\right) N_i + N_i N_j} \Phi^e_{\sum out/in}. \tag{65}$$

The Johnson's length, Λ (m), is a petrophysical parameter proposed by *Schwartz et al.* [1989] that quantifies a representative length of a porous medium. Following *Bernabé and Revil* [1995], we computed two Johnson's lengths for each of our networks:

$$\Lambda_h = \frac{\sum_{i=1}^{N_t} R_i^2 |\Delta P_i|^2}{\sum_{i=1}^{N_t} R_i |\Delta P_i|}. \tag{66}$$

and

$$\Lambda_e = \frac{\sum_{i=1}^{N_t} R_i^2 |\Delta V_i|^2}{\sum_{i=1}^{N_t} R_i |\Delta V_i|}. \tag{67}$$

where N_t is the total number of nodes and ΔP_i (resp. ΔV_i) is the gradient of hydraulic pressure (resp. electrical potential) between the two ends of capillary I (of radius R_i). By definition, the hydraulic and electrical Johnson's lengths are based on the hydraulic (Eq. 66) and the electrical potentials (Eq. 67), respectively. These two lengths are expected to have close values.

Appendix C: Simulation results

This table regroups all the numerical results from the simulation of the present study for the different types of pore size distributions: fractal (Fract.), exponential symmetric (Exp. Sym.), lognormal (Log.), and double lognormal (Dbl. Log.).

Type	R range (μm)	C^w_{NaCl} (mol/L)	C_{EK} (mV/m)	k/phi (mD)	$F \times phi$ (-)	σ_w (S/m)	$\hat{Q}_v$ (C/m^3)	Λ_h (μm)	Λ_e (μm)
Fract.	0.1-10	0.0001	-140.6379	1.44E-01	23.51	1.09E-03	4.674E+03	0.1337	0.1567
Fract.	0.1-10	0.0005	-52.6636	1.44E-01	23.51	5.42E-03	8.708E+03	0.1337	0.1567
Fract.	0.1-10	0.001	-29.6833	1.44E-01	23.51	1.08E-02	9.781E+03	0.1337	0.1567
Fract.	0.1-10	0.005	-6.1136	1.44E-01	23.51	5.32E-02	9.914E+03	0.1337	0.1567
Fract.	0.1-10	0.01	-2.8766	1.44E-01	23.51	1.05E-01	9.219E+03	0.1337	0.1567
Fract.	0.1-10	0.05	-0.4461	1.44E-01	23.51	4.99E-01	6.789E+03	0.1337	0.1567
Fract.	0.1-10	0.1	-0.1902	1.44E-01	23.51	9.61E-01	5.575E+03	0.1337	0.1567
Fract.	0.1-10	0.5	-0.0209	1.44E-01	23.51	4.12E+00	2.626E+03	0.1337	0.1567
Fract.	0.1-10	1	-0.0058	1.44E-01	23.51	7.49E+00	1.331E+03	0.1337	0.1567
Fract.	0.5-50	0.0001	-387.0505	3.60E+00	23.51	1.09E-03	5.146E+02	0.6687	0.7836
Fract.	0.5-50	0.0005	-82.9874	3.60E+00	23.51	5.42E-03	5.489E+02	0.6687	0.7836
Fract.	0.5-50	0.001	-40.1124	3.60E+00	23.51	1.08E-02	5.287E+02	0.6687	0.7836
Fract.	0.5-50	0.005	-6.7928	3.60E+00	23.51	5.32E-02	4.406E+02	0.6687	0.7836
Fract.	0.5-50	0.01	-3.0721	3.60E+00	23.51	1.05E-01	3.938E+02	0.6687	0.7836
Fract.	0.5-50	0.05	-0.4560	3.60E+00	23.51	4.99E-01	2.776E+02	0.6687	0.7836
Fract.	0.5-50	0.1	-0.1929	3.60E+00	23.51	9.61E-01	2.261E+02	0.6687	0.7836
Fract.	0.5-50	0.5	-0.0210	3.60E+00	23.51	4.12E+00	1.056E+02	0.6687	0.7836
Fract.	0.5-50	1	-0.0058	3.60E+00	23.51	7.49E+00	5.344E+01	0.6687	0.7836
Fract.	1-100	0.0001	-461.1766	1.44E+01	23.51	1.09E-03	1.532E+02	1.3374	1.5672
Fract.	1-100	0.0005	-88.5209	1.44E+01	23.51	5.42E-03	1.463E+02	1.3374	1.5672
Fract.	1-100	0.001	-41.7734	1.44E+01	23.51	1.08E-02	1.376E+02	1.3374	1.5672
Fract.	1-100	0.005	-6.8843	1.44E+01	23.51	5.32E-02	1.116E+02	1.3374	1.5672
Fract.	1-100	0.01	-3.0976	1.44E+01	23.51	1.05E-01	9.925E+01	1.3374	1.5672
Fract.	1-100	0.05	-0.4573	1.44E+01	23.51	4.99E-01	6.958E+01	1.3374	1.5672
Fract.	1-100	0.1	-0.1932	1.44E+01	23.51	9.61E-01	5.662E+01	1.3374	1.5672
Fract.	1-100	0.5	-0.0210	1.44E+01	23.51	4.12E+00	2.640E+01	1.3374	1.5672

Fract.	1-100	1	-0.0059	1.44E+01	23.51	7.49E+00	1.336E+01	1.3374	1.5672
Fract.	5-500	0.0001	-539.0909	3.60E+02	23.51	1.09E-03	7.167E+00	6.6872	7.8362
Fract.	5-500	0.0005	-93.3707	3.60E+02	23.51	5.42E-03	6.176E+00	6.6872	7.8362
Fract.	5-500	0.001	-43.1767	3.60E+02	23.51	1.08E-02	5.691E+00	6.6872	7.8362
Fract.	5-500	0.005	-6.9587	3.60E+02	23.51	5.32E-02	4.514E+00	6.6872	7.8362
Fract.	5-500	0.01	-3.1182	3.60E+02	23.51	1.05E-01	3.997E+00	6.6872	7.8362
Fract.	5-500	0.05	-0.4583	3.60E+02	23.51	4.99E-01	2.790E+00	6.6872	7.8362
Fract.	5-500	0.1	-0.1935	3.60E+02	23.51	9.61E-01	2.269E+00	6.6872	7.8362
Fract.	5-500	0.5	-0.0210	3.60E+02	23.51	4.12E+00	1.057E+00	6.6872	7.8362
Fract.	5-500	1	-0.0059	3.60E+02	23.51	7.49E+00	5.348E-01	6.6872	7.8362
Fract.	10-1000	0.0001	-550.3921	1.44E+03	23.51	1.09E-03	1.829E+00	13.3744	15.6723
Fract.	10-1000	0.0005	-94.0061	1.44E+03	23.51	5.42E-03	1.554E+00	13.3744	15.6723
Fract.	10-1000	0.001	-43.3571	1.44E+03	23.51	1.08E-02	1.429E+00	13.3744	15.6723
Fract.	10-1000	0.005	-6.9680	1.44E+03	23.51	5.32E-02	1.130E+00	13.3744	15.6723
Fract.	10-1000	0.01	-3.1208	1.44E+03	23.51	1.05E-01	1.000E+00	13.3744	15.6723
Fract.	10-1000	0.05	-0.4584	1.44E+03	23.51	4.99E-01	6.977E-01	13.3744	15.6723
Fract.	10-1000	0.1	-0.1935	1.44E+03	23.51	9.61E-01	5.672E-01	13.3744	15.6723
Fract.	10-1000	0.5	-0.0210	1.44E+03	23.51	4.12E+00	2.642E-01	13.3744	15.6723
Fract.	10-1000	1	-0.0059	1.44E+03	23.51	7.49E+00	1.337E-01	13.3744	15.6723
Exp. Sym.	0.1-10	0.0001	-413.1205	2.62E+01	4.88	1.09E-03	3.636E+02	0.8264	0.9395
Exp. Sym.	0.1-10	0.0005	-85.0421	2.62E+01	4.88	5.42E-03	3.724E+02	0.8264	0.9395
Exp. Sym.	0.1-10	0.001	-40.7362	2.62E+01	4.88	1.08E-02	3.555E+02	0.8264	0.9395
Exp. Sym.	0.1-10	0.005	-6.8276	2.62E+01	4.88	5.32E-02	2.932E+02	0.8264	0.9395
Exp. Sym.	0.1-10	0.01	-3.0818	2.62E+01	4.88	1.05E-01	2.615E+02	0.8264	0.9395
Exp. Sym.	0.1-10	0.05	-0.4565	2.62E+01	4.88	4.99E-01	1.840E+02	0.8264	0.9395
Exp. Sym.	0.1-10	0.1	-0.1930	2.62E+01	4.88	9.61E-01	1.498E+02	0.8264	0.9395
Exp. Sym.	0.1-10	0.5	-0.0210	2.62E+01	4.88	4.12E+00	6.991E+01	0.8264	0.9395
Exp. Sym.	0.1-10	1	-0.0058	2.62E+01	4.88	7.49E+00	3.539E+01	0.8264	0.9395
Exp. Sym.	0.5-50	0.0001	-525.6708	6.55E+02	4.88	1.09E-03	1.851E+01	4.1317	4.6975
Exp. Sym.	0.5-50	0.0005	-92.5948	6.55E+02	4.88	5.42E-03	1.622E+01	4.1317	4.6975
Exp. Sym.	0.5-50	0.001	-42.9554	6.55E+02	4.88	1.08E-02	1.499E+01	4.1317	4.6975
Exp. Sym.	0.5-50	0.005	-6.9471	6.55E+02	4.88	5.32E-02	1.193E+01	4.1317	4.6975
Exp. Sym.	0.5-50	0.01	-3.1150	6.55E+02	4.88	1.05E-01	1.057E+01	4.1317	4.6975

Exp. Sym.	0.5-50	0.05	-0.4581	6.55E+02	4.88	4.99E-01	7.386E+00	4.1317	4.6975
Exp. Sym.	0.5-50	0.1	-0.1934	6.55E+02	4.88	9.61E-01	6.006E+00	4.1317	4.6975
Exp. Sym.	0.5-50	0.5	-0.0210	6.55E+02	4.88	4.12E+00	2.799E+00	4.1317	4.6975
Exp. Sym.	0.5-50	1	-0.0059	6.55E+02	4.88	7.49E+00	1.416E+00	4.1317	4.6975
Exp. Sym.	1-100	0.0001	-543.3634	2.62E+03	4.88	1.09E-03	4.783E+00	8.2635	9.3950
Exp. Sym.	1-100	0.0005	-93.6126	2.62E+03	4.88	5.42E-03	4.099E+00	8.2635	9.3950
Exp. Sym.	1-100	0.001	-43.2455	2.62E+03	4.88	1.08E-02	3.774E+00	8.2635	9.3950
Exp. Sym.	1-100	0.005	-6.9622	2.62E+03	4.88	5.32E-02	2.990E+00	8.2635	9.3950
Exp. Sym.	1-100	0.01	-3.1192	2.62E+03	4.88	1.05E-01	2.647E+00	8.2635	9.3950
Exp. Sym.	1-100	0.05	-0.4583	2.62E+03	4.88	4.99E-01	1.847E+00	8.2635	9.3950
Exp. Sym.	1-100	0.1	-0.1935	2.62E+03	4.88	9.61E-01	1.502E+00	8.2635	9.3950
Exp. Sym.	1-100	0.5	-0.0210	2.62E+03	4.88	4.12E+00	6.997E-01	8.2635	9.3950
Exp. Sym.	1-100	1	-0.0059	2.62E+03	4.88	7.49E+00	3.541E-01	8.2635	9.3950
Exp. Sym.	5-500	0.0001	-558.2680	6.55E+04	4.88	1.09E-03	1.966E-01	41.3174	46.9751
Exp. Sym.	5-500	0.0005	-94.4397	6.55E+04	4.88	5.42E-03	1.654E-01	41.3174	46.9751
Exp. Sym.	5-500	0.001	-43.4797	6.55E+04	4.88	1.08E-02	1.518E-01	41.3174	46.9751
Exp. Sym.	5-500	0.005	-6.9744	6.55E+04	4.88	5.32E-02	1.198E-01	41.3174	46.9751
Exp. Sym.	5-500	0.01	-3.1226	6.55E+04	4.88	1.05E-01	1.060E-01	41.3174	46.9751
Exp. Sym.	5-500	0.05	-0.4585	6.55E+04	4.88	4.99E-01	7.392E-02	41.3174	46.9751
Exp. Sym.	5-500	0.1	-0.1935	6.55E+04	4.88	9.61E-01	6.010E-02	41.3174	46.9751
Exp. Sym.	5-500	0.5	-0.0210	6.55E+04	4.88	4.12E+00	2.799E-02	41.3174	46.9751
Exp. Sym.	5-500	1	-0.0059	6.55E+04	4.88	7.49E+00	1.417E-02	41.3174	46.9751
Exp. Sym.	10-1000	0.0001	-560.1807	2.62E+05	4.88	1.09E-03	4.931E-02	82.6347	93.9501
Exp. Sym.	10-1000	0.0005	-94.5439	2.62E+05	4.88	5.42E-03	4.140E-02	82.6347	93.9501
Exp. Sym.	10-1000	0.001	-43.5092	2.62E+05	4.88	1.08E-02	3.797E-02	82.6347	93.9501
Exp. Sym.	10-1000	0.005	-6.9759	2.62E+05	4.88	5.32E-02	2.996E-02	82.6347	93.9501
Exp. Sym.	10-1000	0.01	-3.1230	2.62E+05	4.88	1.05E-01	2.650E-02	82.6347	93.9501
Exp. Sym.	10-1000	0.05	-0.4585	2.62E+05	4.88	4.99E-01	1.848E-02	82.6347	93.9501
Exp. Sym.	10-1000	0.1	-0.1935	2.62E+05	4.88	9.61E-01	1.502E-02	82.6347	93.9501
Exp. Sym.	10-1000	0.5	-0.0210	2.62E+05	4.88	4.12E+00	6.998E-03	82.6347	93.9501
Exp. Sym.	10-1000	1	-0.0059	2.62E+05	4.88	7.49E+00	3.541E-03	82.6347	93.9501
Log.	0.1-10	0.0001	-410.0958	2.88E+01	4.51	1.09E-03	3.554E+02	0.7898	0.9386
Log.	0.1-10	0.0005	-84.7976	2.88E+01	4.51	5.42E-03	3.656E+02	0.7898	0.9386

Log.	0.1-10	0.001	-40.6616	2.88E+01	4.51	1.08E-02	3.493E+02	0.7898	0.9386
Log.	0.1-10	0.005	-6.8234	2.88E+01	4.51	5.32E-02	2.885E+02	0.7898	0.9386
Log.	0.1-10	0.01	-3.0807	2.88E+01	4.51	1.05E-01	2.574E+02	0.7898	0.9386
Log.	0.1-10	0.05	-0.4564	2.88E+01	4.51	4.99E-01	1.811E+02	0.7898	0.9386
Log.	0.1-10	0.1	-0.1930	2.88E+01	4.51	9.61E-01	1.475E+02	0.7898	0.9386
Log.	0.1-10	0.5	-0.0210	2.88E+01	4.51	4.12E+00	6.883E+01	0.7898	0.9386
Log.	0.1-10	1	-0.0058	2.88E+01	4.51	7.49E+00	3.484E+01	0.7898	0.9386
Log.	0.5-50	0.0001	-524.7114	7.20E+02	4.51	1.09E-03	1.819E+01	3.9488	4.6930
Log.	0.5-50	0.0005	-92.5376	7.20E+02	4.51	5.42E-03	1.596E+01	3.9488	4.6930
Log.	0.5-50	0.001	-42.9390	7.20E+02	4.51	1.08E-02	1.476E+01	3.9488	4.6930
Log.	0.5-50	0.005	-6.9462	7.20E+02	4.51	5.32E-02	1.175E+01	3.9488	4.6930
Log.	0.5-50	0.01	-3.1148	7.20E+02	4.51	1.05E-01	1.041E+01	3.9488	4.6930
Log.	0.5-50	0.05	-0.4581	7.20E+02	4.51	4.99E-01	7.272E+00	3.9488	4.6930
Log.	0.5-50	0.1	-0.1934	7.20E+02	4.51	9.61E-01	5.914E+00	3.9488	4.6930
Log.	0.5-50	0.5	-0.0210	7.20E+02	4.51	4.12E+00	2.755E+00	3.9488	4.6930
Log.	0.5-50	1	-0.0059	7.20E+02	4.51	7.49E+00	1.394E+00	3.9488	4.6930
Log.	1-100	0.0001	-542.8505	2.88E+03	4.51	1.09E-03	4.704E+00	7.8977	9.3860
Log.	1-100	0.0005	-93.5834	2.88E+03	4.51	5.42E-03	4.035E+00	7.8977	9.3860
Log.	1-100	0.001	-43.2372	2.88E+03	4.51	1.08E-02	3.715E+00	7.8977	9.3860
Log.	1-100	0.005	-6.9618	2.88E+03	4.51	5.32E-02	2.944E+00	7.8977	9.3860
Log.	1-100	0.01	-3.1191	2.88E+03	4.51	1.05E-01	2.606E+00	7.8977	9.3860
Log.	1-100	0.05	-0.4583	2.88E+03	4.51	4.99E-01	1.819E+00	7.8977	9.3860
Log.	1-100	0.1	-0.1935	2.88E+03	4.51	9.61E-01	1.479E+00	7.8977	9.3860
Log.	1-100	0.5	-0.0210	2.88E+03	4.51	4.12E+00	6.889E-01	7.8977	9.3860
Log.	1-100	1	-0.0059	2.88E+03	4.51	7.49E+00	3.486E-01	7.8977	9.3860
Log.	5-500	0.0001	-558.1596	7.20E+04	4.51	1.09E-03	1.935E-01	39.4883	46.9301
Log.	5-500	0.0005	-94.4338	7.20E+04	4.51	5.42E-03	1.629E-01	39.4883	46.9301
Log.	5-500	0.001	-43.4781	7.20E+04	4.51	1.08E-02	1.494E-01	39.4883	46.9301
Log.	5-500	0.005	-6.9743	7.20E+04	4.51	5.32E-02	1.180E-01	39.4883	46.9301
Log.	5-500	0.01	-3.1225	7.20E+04	4.51	1.05E-01	1.044E-01	39.4883	46.9301
Log.	5-500	0.05	-0.4585	7.20E+04	4.51	4.99E-01	7.278E-02	39.4883	46.9301
Log.	5-500	0.1	-0.1935	7.20E+04	4.51	9.61E-01	5.917E-02	39.4883	46.9301
Log.	5-500	0.5	-0.0210	7.20E+04	4.51	4.12E+00	2.756E-02	39.4883	46.9301

Log.	5-500	1	-0.0059	7.20E+04	4.51	7.49E+00	1.395E-02	39.4883	46.9301
Log.	10-1000	0.0001	-560.1261	2.88E+05	4.51	1.09E-03	4.854E-02	78.9766	93.8603
Log.	10-1000	0.0005	-94.5410	2.88E+05	4.51	5.42E-03	4.076E-02	78.9766	93.8603
Log.	10-1000	0.001	-43.5083	2.88E+05	4.51	1.08E-02	3.738E-02	78.9766	93.8603
Log.	10-1000	0.005	-6.9758	2.88E+05	4.51	5.32E-02	2.949E-02	78.9766	93.8603
Log.	10-1000	0.01	-3.1230	2.88E+05	4.51	1.05E-01	2.609E-02	78.9766	93.8603
Log.	10-1000	0.05	-0.4585	2.88E+05	4.51	4.99E-01	1.819E-02	78.9766	93.8603
Log.	10-1000	0.1	-0.1935	2.88E+05	4.51	9.61E-01	1.479E-02	78.9766	93.8603
Log.	10-1000	0.5	-0.0210	2.88E+05	4.51	4.12E+00	6.890E-03	78.9766	93.8603
Log.	10-1000	1	-0.0059	2.88E+05	4.51	7.49E+00	3.487E-03	78.9766	93.8603
Dbl. Log.	0.1-10	0.0001	-294.0487	5.96E+00	17.22	1.09E-03	3.223E+02	0.3398	0.6179
Dbl. Log.	0.1-10	0.0005	-74.1977	5.96E+00	17.22	5.42E-03	4.046E+02	0.3398	0.6179
Dbl. Log.	0.1-10	0.001	-37.3259	5.96E+00	17.22	1.08E-02	4.056E+02	0.3398	0.6179
Dbl. Log.	0.1-10	0.005	-6.6296	5.96E+00	17.22	5.32E-02	3.545E+02	0.3398	0.6179
Dbl. Log.	0.1-10	0.01	-3.0261	5.96E+00	17.22	1.05E-01	3.198E+02	0.3398	0.6179
Dbl. Log.	0.1-10	0.05	-0.4537	5.96E+00	17.22	4.99E-01	2.277E+02	0.3398	0.6179
Dbl. Log.	0.1-10	0.1	-0.1923	5.96E+00	17.22	9.61E-01	1.859E+02	0.3398	0.6179
Dbl. Log.	0.1-10	0.5	-0.0210	5.96E+00	17.22	4.12E+00	8.693E+01	0.3398	0.6179
Dbl. Log.	0.1-10	1	-0.0058	5.96E+00	17.22	7.49E+00	4.403E+01	0.3398	0.6179
Dbl. Log.	0.5-50	0.0001	-482.0907	1.49E+02	17.22	1.09E-03	2.114E+01	1.6989	3.0893
Dbl. Log.	0.5-50	0.0005	-89.9010	1.49E+02	17.22	5.42E-03	1.961E+01	1.6989	3.0893
Dbl. Log.	0.5-50	0.001	-42.1772	1.49E+02	17.22	1.08E-02	1.833E+01	1.6989	3.0893
Dbl. Log.	0.5-50	0.005	-6.9060	1.49E+02	17.22	5.32E-02	1.477E+01	1.6989	3.0893
Dbl. Log.	0.5-50	0.01	-3.1036	1.49E+02	17.22	1.05E-01	1.312E+01	1.6989	3.0893
Dbl. Log.	0.5-50	0.05	-0.4576	1.49E+02	17.22	4.99E-01	9.187E+00	1.6989	3.0893
Dbl. Log.	0.5-50	0.1	-0.1933	1.49E+02	17.22	9.61E-01	7.474E+00	1.6989	3.0893
Dbl. Log.	0.5-50	0.5	-0.0210	1.49E+02	17.22	4.12E+00	3.484E+00	1.6989	3.0893
Dbl. Log.	0.5-50	1	-0.0059	1.49E+02	17.22	7.49E+00	1.763E+00	1.6989	3.0893
Dbl. Log.	1-100	0.0001	-519.4521	5.96E+02	17.22	1.09E-03	5.694E+00	3.3978	6.1785
Dbl. Log.	1-100	0.0005	-92.2258	5.96E+02	17.22	5.42E-03	5.029E+00	3.3978	6.1785
Dbl. Log.	1-100	0.001	-42.8496	5.96E+02	17.22	1.08E-02	4.656E+00	3.3978	6.1785
Dbl. Log.	1-100	0.005	-6.9416	5.96E+02	17.22	5.32E-02	3.712E+00	3.3978	6.1785
Dbl. Log.	1-100	0.01	-3.1135	5.96E+02	17.22	1.05E-01	3.291E+00	3.3978	6.1785

Dbl. Log.	1-100	0.05	-0.4581	5.96E+02	17.22	4.99E-01	2.299E+00	3.3978	6.1785
Dbl. Log.	1-100	0.1	-0.1934	5.96E+02	17.22	9.61E-01	1.870E+00	3.3978	6.1785
Dbl. Log.	1-100	0.5	-0.0210	5.96E+02	17.22	4.12E+00	8.713E-01	3.3978	6.1785
Dbl. Log.	1-100	1	-0.0059	5.96E+02	17.22	7.49E+00	4.409E-01	3.3978	6.1785
Dbl. Log.	5-500	0.0001	-553.0960	1.49E+04	17.22	1.09E-03	2.425E-01	16.9892	30.8926
Dbl. Log.	5-500	0.0005	-94.1557	1.49E+04	17.22	5.42E-03	2.054E-01	16.9892	30.8926
Dbl. Log.	5-500	0.001	-43.3994	1.49E+04	17.22	1.08E-02	1.886E-01	16.9892	30.8926
Dbl. Log.	5-500	0.005	-6.9702	1.49E+04	17.22	5.32E-02	1.491E-01	16.9892	30.8926
Dbl. Log.	5-500	0.01	-3.1214	1.49E+04	17.22	1.05E-01	1.320E-01	16.9892	30.8926
Dbl. Log.	5-500	0.05	-0.4584	1.49E+04	17.22	4.99E-01	9.204E-02	16.9892	30.8926
Dbl. Log.	5-500	0.1	-0.1935	1.49E+04	17.22	9.61E-01	7.483E-02	16.9892	30.8926
Dbl. Log.	5-500	0.5	-0.0210	1.49E+04	17.22	4.12E+00	3.486E-02	16.9892	30.8926
Dbl. Log.	5-500	1	-0.0059	1.49E+04	17.22	7.49E+00	1.764E-02	16.9892	30.8926
Dbl. Log.	10-1000	0.0001	-557.5685	5.96E+04	17.22	1.09E-03	6.111E-02	33.9784	61.7852
Dbl. Log.	10-1000	0.0005	-94.4015	5.96E+04	17.22	5.42E-03	5.148E-02	33.9784	61.7852
Dbl. Log.	10-1000	0.001	-43.4689	5.96E+04	17.22	1.08E-02	4.724E-02	33.9784	61.7852
Dbl. Log.	10-1000	0.005	-6.9738	5.96E+04	17.22	5.32E-02	3.730E-02	33.9784	61.7852
Dbl. Log.	10-1000	0.01	-3.1224	5.96E+04	17.22	1.05E-01	3.300E-02	33.9784	61.7852
Dbl. Log.	10-1000	0.05	-0.4585	5.96E+04	17.22	4.99E-01	2.301E-02	33.9784	61.7852
Dbl. Log.	10-1000	0.1	-0.1935	5.96E+04	17.22	9.61E-01	1.871E-02	33.9784	61.7852
Dbl. Log.	10-1000	0.5	-0.0210	5.96E+04	17.22	4.12E+00	8.715E-03	33.9784	61.7852
Dbl. Log.	10-1000	1	-0.0059	5.96E+04	17.22	7.49E+00	4.410E-03	33.9784	61.7852

Acknowledgments

The authors strongly thank the financial support of ANR EXCITING (Grant No ANR-17-CE06-0012) for this work and for the PhD thesis funding of A. Mendieta. A. Maineult also acknowledges the support of the Russian Science Foundation (Grant No. 17-17-668 01160 'Physical-chemical models of Induced Polarization and Self-Potential with application to pumping test experiments').

References

Bernabé, Y. (1998), Streaming potential in heterogeneous networks, *Journal of Geophysical Research: Solid Earth*, *103*(B9), 20,827–20,841.

Bernabé, Y., and A. Revil (1995), Pore-scale heterogeneity, energy dissipation and the transport properties of rocks, *Geophysical Research Letters*, *22*(12), 1529–1532.

Bolève, A., J. Vandemeulebrouck, and J. Grangeon (2012), Dyke leakage localization and hydraulic permeability estimation through self-potential and hydro-acoustic measurements: Self-potential 'abacus' diagram for hydraulic permeability estimation and uncertainty computation, *Journal of Applied Geophysics*, *86*, 17–28.

Brovelli, A., and G. Cassiani (2010), Sensitivity of intrinsic permeability to electrokinetic coupling in shaly and clayey porous media, *Transport in Porous Media*, *83*(3), 681–697.

Bryant, S., and M. Blunt (1992), Prediction of relative permeability in simple porous media, *Physical review A*, *46*(4), 2004.

Cherubini, A., B. Garcia, A. Cerepi, and A. Revil. (2018), Streaming potential coupling coefficient and transport properties of unsaturated carbonate rocks, *Vadose Zone Journal*, *17*(180030), –, doi:10.2136/vzj2018.02.0030.

Darcy, H. (1856), *Les fontaines publiques de la ville de Dijon: exposition et application...*, Victor Dalmont.

Dullien, F. A. (2012), *Porous media: fluid transport and pore structure*, Academic press.

Fox, R. W. (1830), On the electromagnetic properties of metalliferous veins in the mines of cornwall., *Philosophical Transactions of the Royal Society*, *120*, 399–414.

Glover, P. W., and N. Déry (2010), Streaming potential coupling coefficient of quartz glass bead packs: Dependence on grain diameter, pore size, and pore throat radius, *Geophysics*, *75*(6), F225–F241.

Gonçalvès, J., P. Rousseau-Gueutin, and A. Revil (2007), Introducing interacting diffuse layers in tlm calculations: A reappraisal of the influence of the pore size on the swelling pressure and the osmotic efficiency of compacted bentonites, *Journal of colloid and interface science*, *316*(1), 92–99.

Guarracino, L., and D. Jougnot (2018), A physically based analytical model to describe effective excess charge for streaming potential generation in water saturated porous media, *Journal of Geophysical Research: Solid Earth*, *123*(1), 52–65.

Guarracino, L., T. Rötting, and J. Carrera (2014), A fractal model to describe the evolution of multiphase flow properties during mineral dissolution, *Advances in Water Resources*, *67*, 78–86.

Helmholtz, H. V. (1879), Studien über electrische grenzschichten, *Annalen der Physik*, *243*(7), 337–382.

Hiemstra, T., and W. H. Van Riemsdijk (2006), On the relationship between charge distribution, surface hydration, and the structure of the interface of metal hydroxides, *Journal of Colloid and Interface Science*, *301*(1), 1–18.

Hunter, R. (1981), *Zeta Potential in Colloid Science: Principles and Applications*, Colloid Science Series, Academic Press.

Jaafar, M. Z., J. Vinogradov, and M. D. Jackson (2009), Measurement of streaming potential coupling coefficient in sandstones saturated with high salinity nacl brine, *Geophysical Research Letters*, *36*(21), n/a–n/a, doi:10.1029/2009GL040549, l21306.

Jackson, M. D. (2008), Characterization of multiphase electrokinetic coupling using a bundle of capillary tubes model, *Journal of Geophysical Research*, *113*(B4).

Jackson, M. D. (2010), Multiphase electrokinetic coupling: Insights into the impact of fluid and charge distribution at the pore scale from a bundle of capillary tubes model, *Journal of Geophysical Research*, *115*, doi:10.1029/2009JB007092.

Jardani, A., and A. Revil (2009), Stochastic joint inversion of temperature and self-potential data, *Geophysical Journal International*, *179*(1), 640–654.

Jardani, A., A. Revil, A. Bolève, A. Crespy, J. Dupont, W. Barrash, and B. Malama (2007), Tomography of the darcy velocity from self-potential measurements, *Geophysical Research Letters*, *34*(24), L24,403.

Jougnot, D., N. Linde, A. Revil, and C. Doussan (2012), Derivation of soil-specific streaming potential electrical parameters from hydrodynamic characteristics of partially saturated soils, *Vadose Zone Journal*, *11*(1).

Jougnot, D., J. G. Rubino, M. Rosas-Carbajal, N. Linde, and K. Holliger (2013), Seismoelectric effects due to mesoscopic heterogeneities, *Geophysical Research Letters*, *40*(10), 2033–2037, doi:10.1002/grl.50472.

Jougnot, D., N. Linde, E. Haarder, and M. Looms (2015), Monitoring of saline tracer movement with vertically distributed self-potential measurements at the HOBE agricultural test site, voulund, denmark, *Journal of Hydrology*, *521*(0), 314 – 327, doi: http://dx.doi.org/10.1016/j.jhydrol.2014.11.041.

730 Jouniaux, L., and J. Pozzi (1995a), Streaming potential and permeability of saturated sand-
731 stones under triaxial stress: Consequences for electrotelluric anomalies prior to earth-
732 quakes, *Journal of Geophysical Research: Solid Earth*, *100*(B6), 10,197–10.
733 Jouniaux, L., and J. Pozzi (1995b), Permeability dependence of streaming potential in
734 rocks for various fluid conductivities, *Geophysical Research Letters*, *22*(4), 485–488.
735 Jouniaux, L., A. Maineult, V. Naudet, M. Pessel, and P. Sailhac (2009), Review of self-
736 potential methods in hydrogeophysics, *Comptes Rendus Geosciences*, *341*(10-11), 928–
737 936.
738 Kirchhoff, S. (1845), Ueber den durchgang eines elektrischen stromes durch eine ebene,
739 insbesondere durch eine kreisförmige, *Annalen der Physik*, *140*(4), 497–514.
740 Kormiltsev, V. V., A. N. Ratushnyak, and V. A. Shapiro (1998), Three-dimensional model-
741 ing of electric and magnetic fields induced by the fluid flow movement in porous media,
742 *Physics of the earth and planetary interiors*, *105*(3), 109–118.
743 Leroy, P., and A. Maineult (2018), Exploring the electrical potential inside cylinders be-
744 yond the debye–hückel approximation: a computer code to solve the poisson–boltzmann
745 equation for multivalent electrolytes, *Geophysical Journal International*, *214*(1), 58–69.
746 Leroy, P., and A. Revil (2004), A triple-layer model of the surface electrochemical proper-
747 ties of clay minerals, *Journal of Colloid and Interface Science*, *270*(2), 371–380.
748 Leroy, P., D. Jougnot, A. Revil, A. Lassin, and M. Azaroual (2012), A double layer model
749 of the gas bubble/water interface, *Journal of Colloid and Interface Science*, *388*(1), 243–
750 256.
751 Leroy, P., N. Devau, A. Revil, and M. Bizi (2013), Influence of surface conductivity on
752 the apparent zeta potential of amorphous silica nanoparticles, *Journal of Colloid and*
753 *Interface Science*, *410*, 81–93.
754 Leroy, P., C. Tournassat, O. Bernard, N. Devau, and M. Azaroual (2015), The elec-
755 trophoretic mobility of montmorillonite. zeta potential and surface conductivity effects,
756 *Journal of colloid and interface science*, *451*, 21–39.
757 Li, S., P. Leroy, F. Heberling, N. Devau, D. Jougnot, and C. Chiaberge (2016), Influence
758 of surface conductivity on the apparent zeta potential of calcite, *Journal of colloid and*
759 *interface science*, *468*, 262–275.
760 Linde, N. (2009), Comment on "characterization of multiphase electrokinetic coupling
761 using a bundle of capillary tubes model" by mathew d. jackson, *Journal of Geophysical*
762 *Research*, *114*(B6), B06,209.

763 Linde, N., A. Revil, A. Boleve, C. Dagès, J. Castermant, B. Suski, and M. Voltz (2007),
764 Estimation of the water table throughout a catchment using self-potential and piezomet-
765 ric data in a bayesian framework, *Journal of Hydrology*, *334*(1), 88–98.
766 Linde, N., J. Doetsch, D. Jougnot, O. Genoni, Y. Dürst, B. Minsley, T. Vogt, N. Pasquale,
767 and J. Luster (2011), Self-potential investigations of a gravel bar in a restored river cor-
768 ridor, *Hydrology and Earth System Sciences*, *15*(3), 729–742.
769 Maineult, A., A. Revil, C. Camerlynck, N. Florsch, and K. Titov (2017), Upscaling of
770 spectral induced polarization response using random tube networks, *Geophysical Jour-*
771 *nal International*, *209*(2), 948–960.
772 Maineult, A., D. Jougnot, and A. Revil (2018), Variations of petrophysical properties and
773 spectral induced polarization in response to drainage and imbibition: a study on a corre-
774 lated random tube network, *Geophysical Journal International*, *212*(2), 1398–1411.
775 McCleskey, R. B. (2011), Electrical conductivity of electrolytes found in natural waters
776 from (5 to 90) c, *Journal of Chemical & Engineering Data*, *56*(2), 317–327.
777 Monachesi, L. B., J. G. Rubino, M. Rosas-Carbajal, D. Jougnot, N. Linde, B. Quintal, and
778 K. Holliger (2015), An analytical study of seismoelectric signals produced by 1-d meso-
779 scopic heterogeneities, *Geophysical Journal International*, *201*(1), 329–342.
780 Morgan, F., E. Williams, and T. Madden (1989), Streaming potential properties of west-
781 erly granite with applications, *Journal of Geophysical Research: Solid Earth*, *94*(B9),
782 12,449–12,461.
783 Nourbehecht, B. (1963), Irreversible thermodynamic effects in inhomogeneous media and
784 their applications in certain geoelectric problems, Ph.D. thesis, Massachusetts Institute
785 of Technology.
786 Obliger, A., M. Jardat, D. Coelho, S. Bekri, and B. Rotenberg (2014), Pore network model
787 of electrokinetic transport through charged porous media, *Physical Review E*, *89*(4),
788 043,013.
789 Pengra, D. B., S. Xi Li, and P.-z. Wong (1999), Determination of rock properties by low-
790 frequency ac electrokinetics, *Journal of Geophysical Research: Solid Earth*, *104*(B12),
791 29,485–29,508.
792 Pride, S. R., and F. Morgan (1991), Electrokinetic dissipation induced by seismic waves,
793 *Geophysics*, *56*(7), 914–925.
794 Quincke, G. (1859), Ueber eine neue art elektrischer ströme, *Annalen der Physik*, *183*(5),
795 1–47.

Revil, A. (2017), Comment on dependence of shear wave seismoelectrics on soil textures: a numerical study in the vadose zone by f.i. zyserman, l.b. monachesi and l. jouniaux, *Geophysical Journal International*, *209*(2), 1095, doi:10.1093/gji/ggx078.

Revil, A., and L. Cathles (1999), Permeability of shaly sands, *Water Resources Research*, *35*(3), 651–662.

Revil, A., and A. Jardani (2013), *The Self-Potential Method: Theory and Applications in Environmental Geosciences*, Cambridge University Press.

Revil, A., and P. Leroy (2004), Constitutive equations for ionic transport in porous shales, *Journal of Geophysical Research*, *109*(B3), B03,208.

Revil, A., P. Pezard, and P. Glover (1999a), Streaming potential in porous media: 1. theory of the zeta potential, *Journal of Geophysical Research: Solid Earth*, *104*(B9), 20,021–20,031.

Revil, A., H. Schwaeger, L. Cathles, and P. Manhardt (1999b), Streaming potential in porous media: 2. theory and application to geothermal systems, *Journal of Geophysical Research: Solid Earth*, *104*(B9), 20,033–20,048.

Revil, A., N. Linde, A. Cerepi, D. Jougnot, S. Matthäi, and S. Finsterle (2007), Electrokinetic coupling in unsaturated porous media, *Journal of Colloid and Interface Science*, *313*(1), 315–327.

Revil, A., A. Jardani, P. Sava, and A. Haas (2015), *The Seismoelectric Method: Theory and Application*, John Wiley & Sons.

Roubinet, D., N. Linde, D. Jougnot, and J. Irving (2016), Streaming potential modeling in fractured rock: Insights into the identification of hydraulically active fractures, *Geophysical Research Letters*, *43*(10), 4937–4944.

Schwartz, L. M., P. N. Sen, and D. L. Johnson (1989), Influence of rough surfaces on electrolytic conduction in porous media, *Physical Review B*, *40*(4), 2450.

Sen, P. N., and P. A. Goode (1992), Influence of temperature on electrical conductivity on shaly sands, *Geophysics*, *57*(1), 89–96.

Sill, W. R. (1983), Self-potential modeling from primary flows, *Geophysics*, *48*(1), 76–86.

Soldi, M., D. Jougnot, and L. Guarracino (2019), An analytical effective excess charge density model to predict the streaming potential generated by unsaturated flow, *Geophysical Journal International*, *216*(1), 380–394.

Soueid Ahmed, A., A. Jardani, A. Revil, and J. Dupont (2014), Hydraulic conductivity field characterization from the joint inversion of hydraulic heads and self-potential data,

Water Resources Research, *50*(4), 3502–3522.

Sverjensky, D. A. (2006), Prediction of the speciation of alkaline earths adsorbed on mineral surfaces in salt solutions, *Geochimica et Cosmochimica Acta*, *70*(10), 2427–2453.

Thanh, L. D. (2018), Effective excess charge density in water saturated porous media, *VNU Journal of Science: Mathematics - Physics*, *34*(4), doi:10.25073/2588-1124/vnumap.4294.

Titov, K., Y. Ilyin, P. Konosavski, and A. Levitski (2002), Electrokinetic spontaneous polarization in porous media: petrophysics and numerical modelling, *Journal of Hydrology*, *267*(3–4), 207 – 216, doi:http://dx.doi.org/10.1016/S0022-1694(02)00151-8.

Tyler, S. W., and S. W. Wheatcraft (1990), Fractal processes in soil water retention, *Water Resources Research*, *26*(5), 1047–1054.

von Smoluchowski, M. (1903), Contribution to the theory of electro-osmosis and related phenomena, *Bull Int Acad Sci Cracovie*, *3*, 184–199.

Winsauer, W. O., H. Shearin Jr, P. Masson, and M. Williams (1952), Resistivity of brine-saturated sands in relation to pore geometry, *AAPG bulletin*, *36*(2), 253–277.

Yu, B., J. Li, Z. Li, and M. Zou (2003), Permeabilities of unsaturated fractal porous media, *International journal of multiphase flow*, *29*(10), 1625–1642.

Zhang, W., J. Yao, Y. Gao, Q. Zhang, and H. Sun (2015), Analysis of electrokinetic coupling of fluid flow in porous media using a 3-d pore network, *Journal of Petroleum Science and Engineering*, *134*, 150–157.